

INTEGRATION OF A LATERAL FLOW IMMUNOASSAY PANEL FOR
GASTROENTERITIS WITH SWAB-BASED SAMPLE
PREPARATION CARTRIDGE

By

Zhenyuan Lu, B.E.

A thesis submitted to the Graduate Council of
Texas State University in partial fulfillment
of the requirements for the degree of
Master of Science
with a Major in Biology
May 2017

Committee Members:

Shannon E. Weigum, Chair

John C. Carrano

Rodney E. Rohde

COPYRIGHT

by

Zhenyuan Lu

2017

FAIR USE AND AUTHOR'S PERMISSION STATEMENT

Fair Use

This work is protected by the Copyright Laws of the United States (Public Law 94-553, section 107). Consistent with fair use as defined in the Copyright Laws, brief quotations from this material are allowed with proper acknowledgement. Use of this material for financial gain without the author's express written permission is not allowed.

Duplication Permission

As the copyright holder of this work I, Zhenyuan Lu, refuse permission to copy in excess of the "Fair Use" exemption without my written permission.

ACKNOWLEDGEMENTS

Foremost, I would like to thank my advisor Dr. Weigum for the continuous support of my M.S. study. She gave me a lot of suggestions on my thesis research with great patience. Every single time, when I face a challenge, she always encourages me to hang in there and overcome the difficulties to reach the goal. I have learned a lot from her.

Besides my advisor, I would like to thank Dr. John C. Carrano for offering me the internship opportunity at Paratus Diagnostics, LLC and leading me to work on the point-of-care project which also related to my thesis. Dr. Rodney E. Rohde, for his encouragement, support and patience.

I also thank my fellow labmate in Dr. Weigum's lab: Kshitij Ranjan who assisted me with the dose-response experiment, data collection and figure assembly and for the sleepless night we were working together on the dose-response experiment; and Katie Kendrick, for the inspired discussions.

Last but not the least, I would like to thank my parents, Jianping Lu and Yiwen He, who gave birth to me and support my life, my decisions...everything!

TABLE OF CONTENTS

	Page
ACKNOWLEDGEMENTS.....	iv
LIST OF FIGURES	vii
ABSTRACT.....	x
CHAPTER	
1. INTRODUCTION	1
1.1. Statistics and Impact of Gastroenteritis (GE) Worldwide	1
1.2. Existing Diagnostic Methods for GE.....	2
1.2.1. Microscopy	2
1.2.2. Specimen Culture.....	3
1.2.3. Molecular Tests.....	3
1.2.4. Antigen-based Detection.....	6
1.3. Challenges for GE Diagnostics in Developing Countries.....	7
1.4. Lateral Flow and Other Low-cost Diagnostic Platforms for Use at the Point-of-Care	8
1.5. Thesis overview	9
2. DESIGN AN LFIA STRIP TO FIT THE TWO-STAGE PARATUSSDS [®] CARTRIDGE.....	12
2.1. Overview	12
2.2. Experimental Methods.....	13
2.2.1. Materials and Reagents	13
2.2.2. Prototype Design and Approaches.....	15
2.2.3. Array Spotting of Immunoassay Capture Reagents.....	18
2.2.4. Norovirus Detection in LFIA Strip – Impact of NC Material and Flow Rate.....	20
2.2.5. Integrated Assays	21
2.3. Results and Discussions.....	24

2.3.1. Optimization of Spotting Parameters and Material Flow Rate.....	24
2.3.2. Norovirus Detection in LFIA Strips	26
2.3.3. Combination of ParatusSDS [®] Cartridge and Norovirus LFIA Assay	28
3. DESIGN FULLY INTEGRATED LFIA STRUCTURE WITH SECOND-GENERATION PARATUSSDS [®] CARTRIDGE.....	35
3.1. Timed Delivery - Network Design for Multistep Assays	35
3.1.1. 2-Dimension Geometry-Based Programmable Network	35
3.1.2. 3-Dimension Geometry-Based Programmable Network	46
3.1.3. Combination of 2-Dimensions and 3-Dimensions Control Strategies.....	55
4. CONCLUSIONS AND FUTURE DIRECTIONS.....	67
REFERENCES	69

LIST OF FIGURES

Figure	Page
1. The traditional lateral flow immunoassay device	9
2. Illustration of the two-stage ParatusSDS® Cartridge and paper-based LFIA strip insert.....	12
3. Prototype LFIA for the two-stage ParatusSDS® Cartridge.....	15
4. (a) Scale drawing of the four prototype μ PAD components	16
5. Schematic of the 3 x 3 array layout within the reaction area of the prototype LFIA strip including a goat anti-mouse control antibody, anti-PBP2a, anti-Cryptosporidium, anti- Giardia, anti-norovirus GII.4, anti-norovirus GI and anti-rotavirus (top-bottom/left-right)	18
6. Example nitrocellulose strip printed with 2-50 nL BSA and stained using Panceau S	24
7. Effect of nitrocellulose material and flow rate on array patterning	25
8. Measured spot diameters in various nitrocellulose materials	26
9. Comparison the signal intensity among 75sec/4cm, 135sec/4cm and 180sec/4cm.....	27
10. Integrated LFIA assay for Norovirus with the ParatusSDS® Cartridge.....	29
11. Dose-response data and curve for integrated μ PAD Norovirus assays with Paratus SDS® Cartridge	30
12. A high dose hook is observed in the plotted curve when high antigen concentration has been introduced into an immunoassay test	31
13. High dose hook effect	31

14. (a) Control group (left, with 0 pM norovirus) shows three dots (incubated by Goat anti-mouse antibody) on the first line (b) Testing group (right) presents a positive signal of norovirus on the second line left dot incubated by 500 pM noroviruses	32
15. The height of the peak presents the intensity of signals showed on the surface of membrane.....	33
16. The signal intensity comparison between the group before gold enhancement treated and after gold enhancement	34
17. Basic network of Multistep paper-based assay panel	35
18. The upper is the prototype version of three inlets structure.....	36
19. Inline network test.....	38
20. Inline network test.....	38
21. 3D printed device for measuring serpentine structure actuation time	40
22. The length-dependent experiment of glass fiber.....	41
23. The plot shows length of strips from 0mm to 50mm vs. the time	41
24. The plot shows length of strips from 0mm to 50mm vs. the square root of time	42
25. Fluids traverse through into the nitrocellulose membrane during the wet-out process in uniform-width and sudden-expansion channels	43
26. Fluids traverse through into the nitrocellulose membrane during the wet-out process in uniform-width and sudden-contraction channels.....	44
27. The side view of programmable fluidic driven network.....	46
28. The side view of holding chamber V1 and V2	49
29. Holding chamber V2.2.....	50
30. The actuation time of two groups of FDT	52

31. The length of neck of FDT in a fixed width of neck V.S. actuation time.....	53
32. *Overall length 50mm, neck width in 4, 5, 6 and no neck, success rate for all is 0% (n=8) ** The group of overall lengths of 60mm w/o neck success rate is 37.5%, average time: 187.6 secs (n=8)	54
33. Prototype V1 Serpentine-based-fluidic-driven network and V1 programmable timing device.....	55
34. Prototype V2 Serpentine-based-fluidic-driven network and V2 programmable timing device.....	57
35. Prototype V3 Serpentine-based-fluidic-driven network and V3 programmable timing device.....	59
36. Prototype V4 Serpentine-based-fluidic-driven network and V4 programmable timing device.....	61
37. Prototype V5 Serpentine-based-fluidic-driven network and V5 programmable timing device.....	63
38. Prototype V6 Serpentine-based-fluidic-driven network and V6 programmable timing device.....	64
39. The dose-response experiment for Norovirus GII.4 (n=2)	65

ABSTRACT

Gastroenteritis is one of the most common and deadly diseases, causing a combination of diarrhea, vomiting, and abdominal pain. In developing countries, there is a lack of advanced medical instruments, well-trained medical personnel and funding to process complex diagnostic tests that inform treatment decisions. Therefore, there is a need to develop inexpensive, easy-to-use, rapid, portable and highly sensitive detection assays that do not require a complex testing procedure or highly trained personnel. To address this need, we have developed of a novel lateral flow immunoassay (LFIA) that uses colorimetric signal enhancement of gold nanoparticles (AuNP) that can be integrated with a point-of-care, swab-based sample preparation cartridge, known as the *Paratus SDS[®] Cartridge* (Paratus Diagnostics, LLC. Austin, TX). These LFIA devices were fabricated using a combination of laser cutting and wax printing to create physical or hydrophobic barriers that directly metered volumes of sample fluids extracted from the *Paratus SDS[®] Cartridge* onto the LFIA test strip. Capillary action was used to draw fluids toward the reaction zone where embedded multiplex immunoassay reagents were embedded in a 3 x 3 microarray spot pattern. In the presence of the target pathogen, a sandwich based immunoassay complex formed between the capture antibody, pathogen, and detecting antibody, yielding a spatially resolved colorimetric signal. Assay results using a single pathogen, Norovirus GII.4 virus-like particles (VLPs), yielded visible AuNP signals in the presence of as little as 50 pM VLP protein using this 2-stage

integrated sample prep/detection system. However, with true point-of-care systems, minimal user interaction is necessary, therefore, we refined the LFIA design to accommodate a one-button *Paratus SDS[®] Cartridge* that operates with a single actuation step which triggers timed delivery of multiple immunoassay reagents and signal enhancers for high sensitivity pathogen detection. This thesis describes the evolution of the LFIA design, theoretical and experimental basis for timed delivery in capillary-driven microfluidic networks, and integration into the *Paratus SDS[®] Cartridge*.

1. INTRODUCTION

1.1. Statistics and Impact of Gastroenteritis (GE) Worldwide

Worldwide, the number of gastroenteritis cases that occur each year is estimated from three to five billion, resulting in roughly 1.4 million deaths, primarily among children located in developing countries (Elliott, 2007; Lozano *et al.*, 2012; Webber, 2005). In these areas, children under two years of age frequently get six or more infections a year resulting in significantly higher morbidity and mortality than those in developed countries (Mandell *et al.*, 2010). Even in the developed world, the rate of intestinal infections remains high (with approximately 100 million cases in the United States) and is currently a serious clinical problem (Casburn-Jones & Farthing, 2004). For instance, in the United States, there are about ~10% of gastroenteritis cases that require hospitalization annually, with over 1.5 million outpatient visits and around 300 deaths in children under five years related to diarrheal illness (Webber, 2005). Unfortunately, few cases in either developed or developing countries undergo a definitive diagnosis to trace the cause of illness to a pathogenic bacterium, virus, or protozoan parasite, or other cause (Casburn-Jones & Farthing, 2004; Gill *et al.*, 2003). When diagnostic stool tests are ordered, they often suffer from limited sensitivity (Iijima *et al.*, 2007; Jamison, 2006 ; Pawlowski *et al.*, 2009) and require significant investments in time and personnel (Sidoti *et al.*, 2015). Since treatment decisions are dependent upon the etiologic agent, for instance, viral causes are not effectively treated with antibiotics (*Antibiotics Aren't Always the Answer*, 2015) accurate diagnosis of gastroenteritis is essential in order to provide proper treatment and prevention.

1.2. Existing Diagnostic Methods for GE

There are four common methods for detecting pathogens causing GE. They are microscopy, culture, molecular detection, and antigen-based immunoassays. The pros and cons of each method are discussed below, and some examples of commercially available diagnostic tests are provided in order to give a general overview of existing diagnostic methods.

1.2.1. Microscopy

The use of microscopy (e.g., optical, or electron) for the detection of gastroenteritis is based on the direct visualization of entire viral/bacterial/parasitic particles from the stool of infected patients. Sometimes, immunostaining with fluorescently-tagged target specific antibodies or another stain, such as a gram stain, is used to improve pathogen detection and identification (Hines & Nachamkin, 1996; Holt *et al.*, 1994). Other possible screening tests can also be used to diagnose diarrheal diseases, such as fecal leukocyte test (Hines & Nachamkin, 1996) and fecal lactoferrin marker in identifying intestinal inflammation (SV *et al.*, 2003). While widely accepted, particularly for protozoan pathogens, microscopy typically requires costly instrumentation and is a labor-intensive process that requires skilled technicians and/or pathologists. Detection limits for microscopy-based detection of *Cryptosporidium* (protozoan parasite) have been reported in the range of 1×10^5 microorganisms per mL of watery stool (White, 2010) making this method highly specific but not very sensitive.

1.2.2. Specimen Culture

The application of specimen culture for diagnosing bacterial etiologies is based on the growth of microorganisms from stool samples collected from the infectious individual. Acceptable sample types for culturing bacteria are somewhat limited and include fresh, well-preserved feces or rectal biopsy samples. Culture is further complicated by the fact that for detecting different species, different culture medias need to be applied. For example, non-selective blood agar plates can be used to detect *Aeromonas sp.*, *Plesiomonas shigelloides*, yeasts, *Staphylococcus aureus*, *Pseudomonas aeruginosa*; while xylose lysine deoxycholate agar (XLD) allows growth of *Salmonella* & *Shigella sp*, while inhibiting the growth of family *Enterobacteriaceae*; or Selenite-F media can be used for selective enrichment of *Salmonella spp*. Specimen cultures can yield highly sensitive diagnostic results; however, the long time periods needed for growth typically limit their use at the point-of-care and in developing countries lacking clinical laboratory infrastructure.

1.2.3. Molecular Tests

Molecular tests are based on sequence-specific detection of the microorganism's genetic material (DNA/RNA). Three common methods have been used in the current diagnosis: (1) amplification, (2) hybridization and (3) sequencing and enzymatic digestion of nucleic acids. These methods have recently been reviewed by Dr. Rohde and Dr. Weigum (Rohde & Weigum, 2017) and are briefly discussed below.

Amplification method

One conventional method of amplification is incorporating the amplification of nucleic acids by polymerase chain reaction (PCR) utilizing DNA chain as a template for reaction. The amplification of RNA templates is using reverse transcription-PCR (RT-PCR). One single nucleic acid target is able to be amplified by this method to 10^7 or more copies in one whole reaction. This method involves 20 to 50 cycles. In each cycle, it consists of three sequential reactions. (1) Denaturation of the target is a necessary step, which is necessary for DNA targets, to denature the nucleic acid target into a single strand at a heating temperature of 94°C in a specific thermal cycler. (2) Primer annealing process. Single-stranded primers are designed to anneal specifically to a specific target at the end of the nucleic acid sequence. The annealing reaction is processed under 50°C to 58°C or higher. Such specific temperature based on primer sequences named the melting temperature (T_m) which can be calculated according to the number of A, G, C and T nucleotides within the sequences. (3) The extension of the target. Once the primer annealed to the target sequences, the DNA polymerase is allowed to add nucleotides to the 3' end of each primer which provides the necessary template format for an extension at 72°C . After the accomplishment of PCR, the mixture will be sent to the gel electrophoresis; and the gel will be dyed by ethidium bromide for identification based on the size of amplicons using molecular weight-size markers

Hybridization

Hybridization method is a technique using a recognizable labeled nucleic acid probe known as RNA or DNA can be complementary to a target of a suspected organism causing disease. This method usually can be divided into two categories: nonamplified

and amplified. A nonamplified involves processing in four steps. The probe selection is the first step based on which suspected pathogens are needed to be detected. Then the probe will be mixed with the purified specimen from the patient containing the nucleic acid targets. If an RNA-DNA or DNA-DNA duplex forms between the probe and the target sequence present in the patient specimen, the hybridization assay will present positive result. Otherwise, it shows negative result or the concentration of nucleic acid targets are below the limit of detection of the hybridization assay. Amplified test has an additional step, amplification, to be followed by signal detection.

Sequencing and Enzymatic Digestion of Nucleic Acids

Nucleic acids sequencing is used to determine the whole target sequence taken from an organism. It is different from the above methods only for detecting one part/portion of a specific sequence of the target. Researchers use this method to identify different microbial pathogens, classify unknown pathogens, trace which specific nucleotide gets a mutation or establish the genetic tree of several species deriving from one ancestor. Enzymatic digestion of nucleic acids is processed by using restriction endonucleases. Each of the endonucleases will recognize a short specific target sequence. For example, the different microbial organism can be digested by different endonucleases, which means the sequence's size will be variable. Then, the enzyme will catalyze the digestion of this nucleic acid sequence which will be cut into fragments with specific lengths. Once the nucleic acid sequence has been digested, fragments are moved to gel electrophoresis. This process will separate them based on their weight-size differences. The fragments with the same size will be aggregating in the same band. Then

ethidium bromide will stain all the fragments, which allows them to be visualized under UV light. The results can be analyzed by comparing different banding patterns.

Commercial molecular tests, particularly those that are multiplexed like the BioFire FilmArray™ (BioFire Diagnostics, Salt Lake City, UT) and Luminex xTAG® (Luminex Corp., Austin, TX) GI-panels, are available and offer high sensitivity and specificity; however, the high cost of the instruments and consumables continues to limit their adoption in routine GE diagnostics. For instance, there is a prerequisite to purchasing analytic instruments, Luminex 100/200 or MAGPIX, for reading the sample results on the Luminex GI-panel; meanwhile, the expenditures on maintenance and consumable reagents are needed.

1.2.4. Antigen-based Detection

Antigen-based detection methods rely on the recognition of unique pathogen-specific antigens present in the sample collected from the stool, blood or other resources. Common antigen-based methods include enzyme-linked immunosorbent assays (ELISA) performed in a 96-well plate format and immunochromatographic (IC) strip tests, also known as rapid diagnostic tests (RDT), which utilize lateral flow immunoassays for direct colorimetric detection of target antigens. Advantages of ELISA include high throughput and the ability to obtain quantitative data regarding the amount of antigen present in each patient sample.

On the other hand, RDTs and lateral flow immunoassays (LFIA) have the advantage of being low-cost and easy to use; therefore, they are currently seen as the most amenable technology for point-of-care diagnostics. In fact, several RDTs are commercially available for GI pathogens including SD BIOLINE Norovirus RDT, which

testing time sequence is only 20min. It is much faster than the conventional diagnostic methods, such as molecular test. However, the sensitivity of these tests can be as low as 50-75% (CDC, 2017). Particularly, the Centers for Disease Control and Prevention did not recommend for detecting norovirus infection in sporadic cases of GE by using these commercial RDT (CDC, 2017). Moreover, most tests can only detect one or two pathogens each, such as one of the current commercial RDTs-SD BIOLINE Norovirus RDT which is able to detect Norovirus only. Additionally, the negative results from those commercial RDTs may need to be confirmed by second techniques, such as PCR, due to it may have low specificity. This is not suitable for syndromic diseases such as gastroenteritis that can be caused by a large variety of pathogens.

In summary, the current diagnostic methods may be adequate in most developed countries where well-trained and experienced technicians, highly specialized instruments (e.g. there is a special need for a molecular test to store nucleic acids properly in a special container) and medical infrastructures are all available. However, differential diagnosis of GE pathogens using these existing methods remains a challenge in developing countries which cannot meet these requirements.

1.3. Challenges for GE Diagnostics in Developing Countries

According to the World Health Organization (WHO), 86% of the world's population spends roughly \$6 per capita by year on medical devices (diagnostic equipment or treating instruments, etc.) compared to the developed countries which spend \$290 per capita by year (Nimunkar *et al.*, 2009). Because of this financial limitation, doctors often must make decisions based on clinical symptoms alone without other essential diagnostic information (Nimunkar *et al.*, 2009). Commonly, the low-cost

medical solutions are also not available in developing countries, because there is not enough essential information provided for the medical practitioners to make decisions about treatment (Nimunkar *et al.*, 2009). Furthermore, it is difficult for developing countries to directly implement diagnostic technologies which have been successfully applied in developed countries because they lack hospital infrastructure, well-trained technicians and funding to support proper medical treatment for patients (Chin *et al.*, 2007; Daar *et al.*, 2002; Mabey *et al.*, 2004; Sia *et al.*, 2004; Yager *et al.*, 2006). For instance, in Tanzania, only 15 pathologists (or 1 per 2.5 million people) are present, and 7 of them are located at Tanzania National hospital located in Dodoma (Rambau, 2011). Thus, there remains a critical need to develop effective platforms for infectious disease diagnosis, which can be used in resource-poor settings.

1.4. Lateral Flow and Other Low-cost Diagnostic Platforms for Use at the Point-of-Care

According to WHO, diagnostic instruments for the developing world should meet the ASSURED criteria meaning they should be affordable, sensitive, specific, user-friendly, rapid/robust, equipment free and deliverable to end-users (Peeling *et al.*, 2006). Lateral flow immunoassays (LFIA) (Figure 1) are currently the only commercially available platform which meets these criteria; however, they typically exhibit inadequate sensitivity which can limit their use for many infectious pathogens (Posthuma-Trumpie *et al.*, 2009). Recently, a new class of capillary-driven devices that employ lateral flow techniques, known as microfluidic paper analytical devices (μ PADs) or paper-based microfluidics, have emerged to address these limitations and meet the ASSURED standards for diagnostic assays (Martinez *et al.*, 2010). A variety of low-cost methods has

been described to fabricate μ PADs including wax printing, stamping, and laser cutting (Sharma *et al.*, 2011; Songjaroen *et al.*, 2011). Wax printing is a simple and low-cost method for patterning hydrophobic barriers in the paper that also define un-printed hydrophilic channels or reaction zones (Carrilho *et al.*, 2009). Compared to photolithography, which uses hydrophobic SU-8 photoresist and UV light to build the hydrophobic walls on the paper, wax printing will prevent damaging the flexibility of paper (Songjaroen *et al.*, 2011).

1.5. Thesis overview

The goal of this thesis work was to develop a novel immunoassay platform to examine stool samples collected from gastroenteritis patients that were

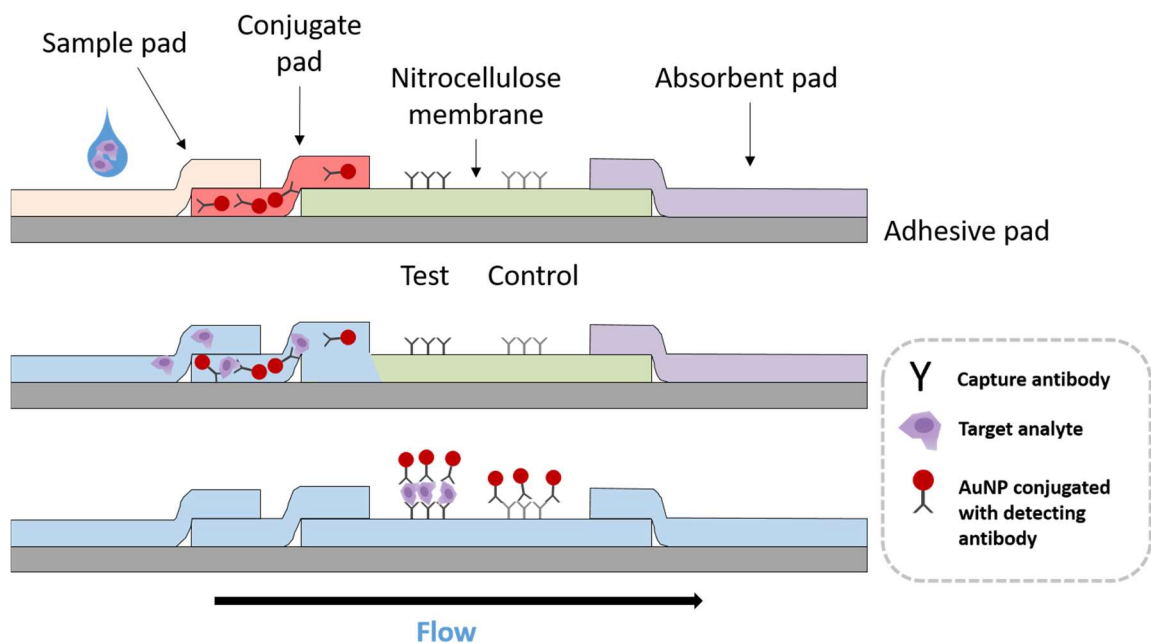


Figure 1. The traditional lateral flow immunoassay device. After the sample contained target analytes have been introduced onto the sample pad, the fluid will flow into the conjugate pad and rehydrate it. Detecting antibody conjugated AuNP will be released and binding with the analytes. When the mobile-complex move through to the reaction area where has been already embedded the capture antibody, the anti-analytes antibody will recognize these complexes and show the positive signal; and the control antibody will recognize the detecting antibody to present if the test work correctly.

concentrated/extracted using the *Paratus SDS*[®] *Cartridge*, then detected on a patterned μ PAD/LFIA strip of paper, which can be multiplexed for detecting several pathogens simultaneously on one device with relatively low cost and minimal user interaction. Unlike the conventional LFIA strip test, our panels were fabricated using a combination of techniques, including wax printing (Xerox[®] Phaser 8640, Xerox Corporation, Norwalk, CT) and by laser cutting (Universal[®] Laser Systems VLS4.60, Universal Laser Systems, Inc., Scottsdale, AZ) of nitrocellulose (NC) and sample/absorbent PAD materials to fit the output/internals of the *Paratus SDS*[®] *Cartridge*. High-affinity immunoreagents, including pathogen-specific antibodies and a positive control, were immobilized within the nitrocellulose membrane by non-contact printing in an array pattern. Raw materials costs remained relatively low, with the cost of the solid ink of wax printer estimated at \sim \\$0.0001/cm² of paper assuming 20% coverage of ink (Peeling *et al.*, 2006; Songjaroen *et al.*, 2011). Generally, the antibodies incubated in the paper are the most expensive component on an LFIA (average \\$300/mg); therefore, reducing the embedded volume of antibodies for each reaction zone was essential for decreasing cost of each device. The BioDot[®] (AD1520, BioDot Inc., Irvine, CA, USA) non-contact aspirator/dispenser instrument was used to precisely dispense antibodies in nanoliter volumes (20 – 50 nL each) onto the nitrocellulose paper, compared to microliter volumes of striped reagents used in common lateral flow assays.

In addition to lowering the cost of diagnostic testing, we addressed the limited LFIA sensitivity through the use of various gold nanoparticle (AuNP) signal enhancement techniques to increase the contrast between colorimetric signals and background noise. Two of these amplification methods included chemical reactions that

nucleate gold or silver ions onto the surface of AuNPs in the presence of a reducing agent, such as hydroquinone (Saha *et al.*, 2012; Sirajuddin *et al.*, 2010).

Taken together, this work aimed to provide an inexpensive, easy-to-use, highly sensitive, sample-to-answer detection system that did not require complex instrumentation or highly trained personnel for differential diagnosis of gastroenteritis. The methods developed here are expected to have widespread application for other assays associated with food or waterborne contamination by infectious pathogens.

2. DESIGN AN LFIA STRIP TO FIT THE TWO-STAGE *PARATUS*SDS[®] *CARTRIDGE*

2.1. Overview

An illustration of the two-stage *Paratus SDS[®] Cartridge* and paper-based LFIA strip insert are shown in Figure 2. Our initial goal was to demonstrate the combined utility of the *Paratus SDS[®] Cartridge* for swab-based sample preparation using Paratus' patented rolling mechanism for extraction of pathogens from a stool sample followed by direct detection of that pathogen in a modified LFIA strip to generate positive/negative signal for appropriate diagnosis.

In this system, the swab is used to collect the sample from a vial of watery stool



Figure 2. Illustration of the two-stage *ParatusSDS[®] Cartridge* and paper-based LFIA strip insert. characteristic of diarrheal illness. Following collection, the swab is inserted into the first chamber of the *ParatusSDS[®] Cartridge*, the lid is closed and the button-like plunger pressed, which flushes an elution buffer through the baffled chamber, thereby extracting

the sample from the swab and delivering it into the second chamber. In the second chamber, the sample is introduced into the LFIA sample pad and wicked through by capillary action to the detection area, which will generate visible colorimetric signals in the presence of target pathogens.

2.2. Experimental Methods

2.2.1. Materials and Reagents

The LFIA devices were designed in Adobe Illustrator CS6 (Adobe System Incorporated, San Jose, CA) and cut from backed nitrocellulose membranes (Hi-Flow Plus 180 Membrane cards, HF180MC100, Millipore Corporation, Billerica, MA), cellulose fiber sample pads (CFSP223000, Millipore Corporation, Billerica, MA) and glass fiber diagnostic pad (GFDX203000, Millipore Corporation, Billerica, MA) using a CO₂ laser (VLS4.60, Universal Laser Systems, Inc., Scottsdale, AZ). Antibodies were obtained from various sources and included: anti-Norovirus GII.4 (#MAB227P and MAB225P, Maine Biotechnology Services, Portland, Maine), and anti-Cryptosporidium (#2402-3007A488, AbD Serotec), as well as anti-Norovirus G1 (#10-1510), anti-Rotavirus (#10-3146), anti-PBP-2a (#10-P08A), and anti-Giardia lamblia (#10-2291) all from Fitzgerald Industries International (Acton, MA). Buffers included phosphate buffered saline (PBS) prepared from BupH Dulbecco's Modified PBS buffer packs (#28374, Thermo Scientific, Waltham, MA) with 0.1% BSA (PBSA, #A3059, Sigma Aldrich, St. Louis, MO), 0.1% Tween-20 (PBST, #P5927, Sigma Adrich) and 0.05%SDS (Bio-Rad Laboratories, Inc, Hercules, CA). Gold nanoparticles were obtained from BBI Solutions (BA. STP40, BBI Solutions, Blaenavon, United Kingdom). Gold enhancement

solutions (GoldEnhance LM, #2112) were sources from Nanoprobes Inc., Yaphank, NY. Biotinylation kits (#21336) were purchased from Thermo Scientific. Virus-like particles (VLPs) was generously provided by Dr. Robert Atmar and Dr. Mary K. Estes from Baylor College of Medicine (Houston, TX).

2.2.2. Prototype Design and Approaches

The first objective was to design a structure to accept fluids extracted using an existing two-stage *ParatusSDS*[®] Cartridge given the cartridge sample elution capacity of 50-100 μL and fixed spatial dimensions. A picture of this prototype is shown in Figure 3.

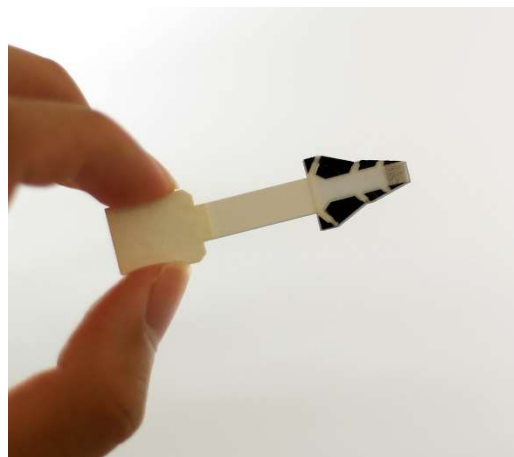


Figure 3. Prototype LFIA for the two-stage *ParatusSDS*[®] Cartridge.

The prototype was fabricated from adhesive nitrocellulose LFIA cards (Hi-Flow[™] Plus, EMD Millipore, Billerica, Massachusetts) with a pyramid-shaped sample inlet laser cut to match the outlet slit dimensions of the *ParatusSDS*[®] Cartridge. Specifications for the prototype design and assembly are shown in Figure 4. This initial LFIA strip consisted of four different parts for several functional purposes, including:

(i) The sample pad (SureWick[®] GFDX 203000), which wicks sample fluid from *ParatusSDS*[®] Cartridge and slowly introduces it onto the nitrocellulose LFIA membrane via capillary action. The total surface area of the sample pad is $0.924 \pm 0.003 \text{ cm}^2$ and was tailored to hold a maximum volume of $55 \mu\text{L}/\text{cm}^2$ when saturated. In addition, we cut the

sample pad into a tree-like structure that could direct fluids, even from the periphery of

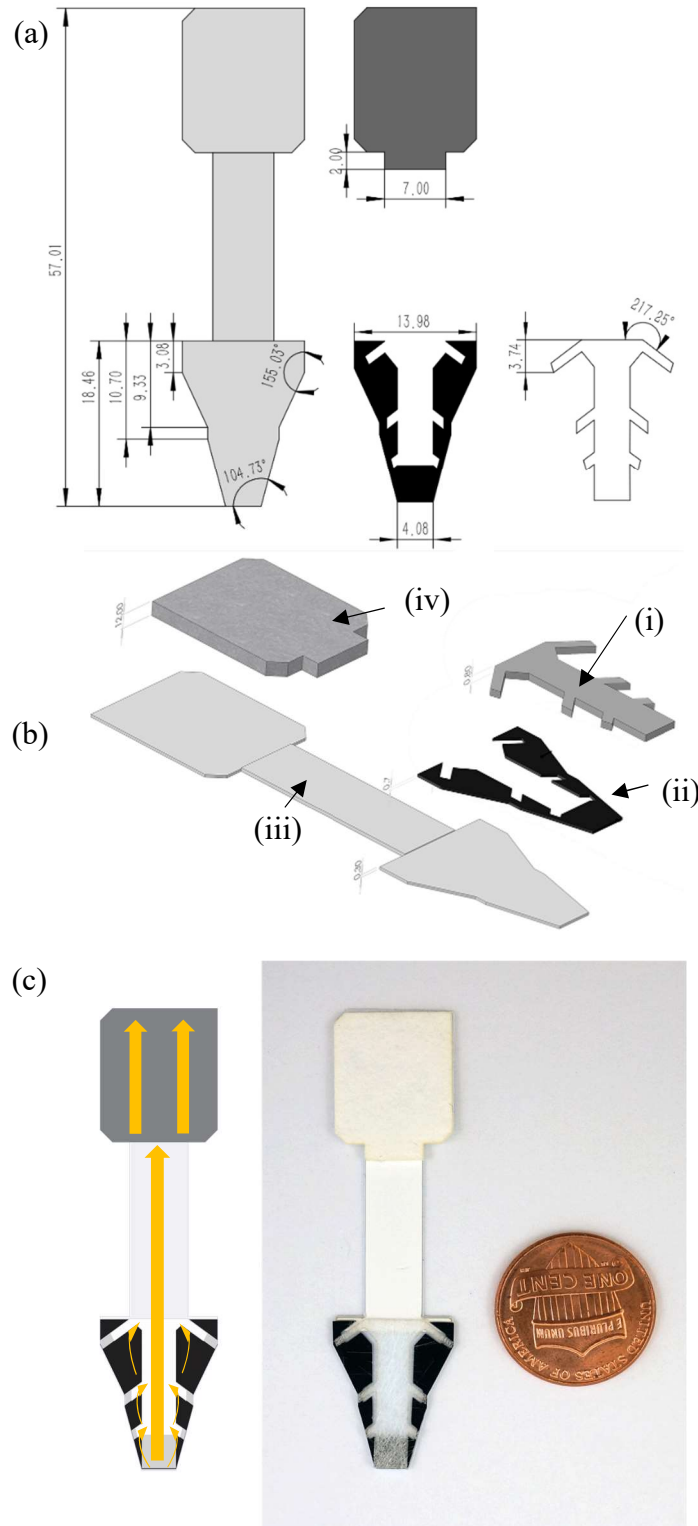


Figure 4. (a) Scale drawing of the four prototype μ PAD components. (b) Three-dimensional schematic of LFIA components and layered assembly onto the LFIA adhesive card. (c) Directional fluid flow pattern (yellow arrows) for the prototype LFIA and scale.

ParatusSDS[®] Cartridge outlet chamber, toward the main fluidic channel in order to ensure collection of all eluted sample onto the LFIA strip.

(ii) The hydrophobic pad serves to restrict fluid from unwanted areas below the sample pad and assist flow toward the tree-like dam and the main channel because there is nowhere else to go.

(iii) The reaction pad consists of the LFIA nitrocellulose membrane with embedded reagents to support sandwich-type immunoassays between capture/detecting antibodies and pathogen-specific antigens. The LFIA membrane is pre-mounted with double-sided adhesives onto a plastic backing, or card, in order to provide additional stability to the otherwise delicate membrane. The adhesive area also allows the sample and absorbent pads to be placed in contact with the nitrocellulose, slightly overlapping on either end, to ensure proper capillary flow.

(iv) The absorbent pad promotes the continuous flow of fluid over the reaction area by capillary action and ensures that the maximum sample volume is analyzed since flow through the full device stops only when the absorbent pad becomes saturated.

2.2.3. Array Spotting of Immunoassay Capture Reagents

Since there are a variety of diverse pathogens that can cause gastroenteritis (i.e. bacteria, protozoan parasites, and viruses), multiplexing is an important piece of any clinically useful diagnostic test. In order to accomplish this task, we used a BioDot

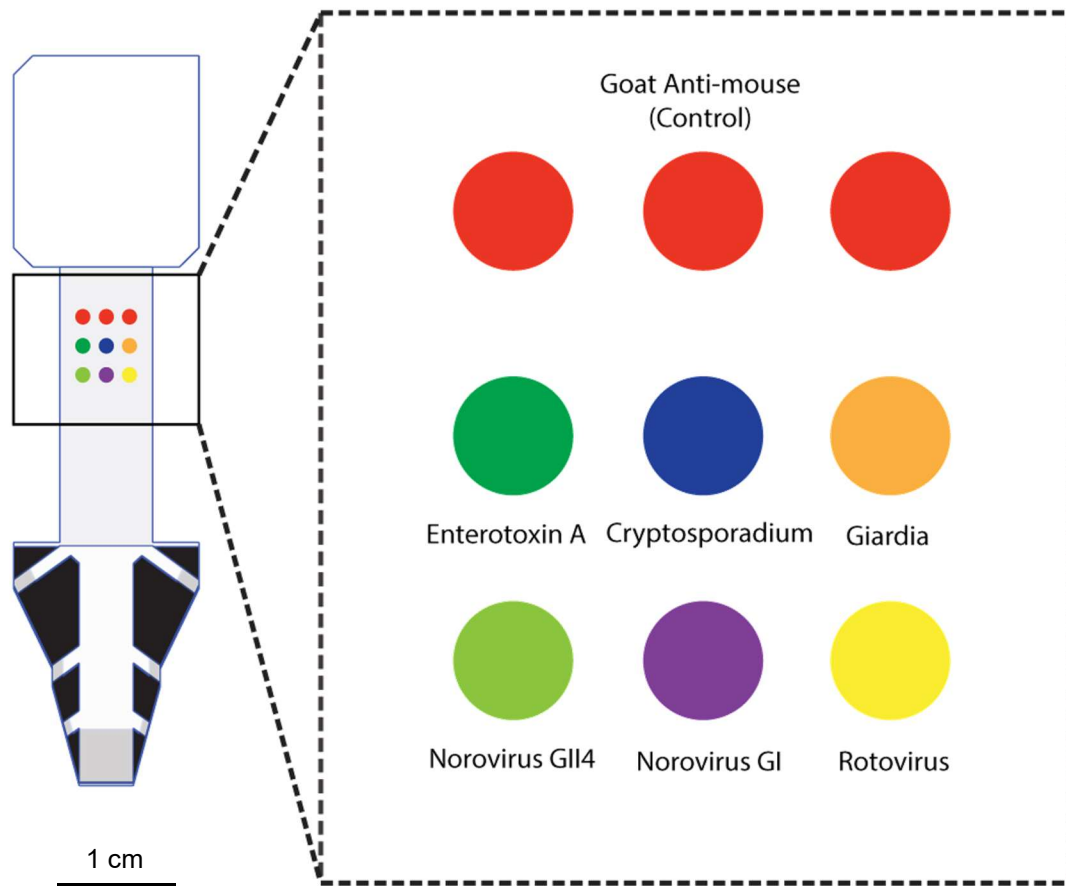


Figure 5. Schematic of the 3 x 3 array layout within the reaction area of the prototype LFIA strip including a goat anti-mouse control antibody, anti-PBP2a, anti-*Cryptosporidium*, anti-*Giardia*, anti-norovirus GII.4, anti-norovirus GI and anti-rotavirus (top-bottom/left-right).

AD1520 (BioDot Inc., Irvine, CA, USA) non-contact, robotic aspirating/dispensing system to print up to 6 different selected target-specific antibodies and 3 replicate controls in a microarray pattern within the LFIA nitrocellulose membrane (reagent area) using a 3 x 3 array layout (Figure 5).

Prior to spotting of the antibodies, we optimized the spotting conditions and nitrocellulose materials (depending upon their porosity and flow rate) in order to obtain discrete, non-overlapping assay spots that could fit within a 7mm nitrocellulose strip. For these experiments, we spotted 250 nL droplets of BSA protein at 1 mg/mL concentration in PBS buffer, dried the membranes at room temperature for 2 hours, and then stained them with Ponceau S (1% in 5% acetic acid) placed in a container for 3min followed by a wash in diH₂O. Nitrocellulose materials tested included HF75, HF135, and HF180 which are characterized by Millipore to contain varying degrees of porosity, and thus varying flow rates and wicking ability. Porosity is a measure of void spaces in a specific material and is calculated according to the equation:

$$\phi = \frac{V_v}{V_T}$$

Where ϕ is the porosity, V_v is volume of void space (e.g. fluids) and V_T is the total volume of material. In these membranes, the lowest porosity, which means with larger void space, is correlated with the highest flow rate (i.e. HF75) and the highest porosity with the slowest flow rate (i.e. HF180).

For antibody spotting, all antibodies were diluted to 0.5 mg/mL – 1 mg/mL in capture buffer (PBS containing 1mg/mL BSA, 0.05% SDS and 2% ethanol) in total volume of 300 μ L and loaded into a 96-well plate. Spotting involved deposition of two 50 nL reagent droplets at the specified locations within the LFIA membranes. Following spotting, the membranes were dried at room temperature or 37°C for a minimum of 1 hr., then stored in a plastic container with desiccant to control humidity for up to two weeks.

2.2.4. Norovirus Detection in LFIA Strip – Impact of NC Material and Flow Rate

Cutting Protocol

- 1) Launched the exhaust system with the round button.
- 2) Logged in the computer and opened the Universal Control Panel (UCP).
- 3) Powered on the laser with the white button.
- 4) Focused the laser to the nitrocellulose membrane.
- 5) Positioned the acrylic window (holding tool for getting the NC membrane in an accurate position) both edges against the rulers. The top edge of the NC membrane card needed to be aligned with two markers of the acrylic window, which meant the NC membrane card has been set in a right location.
- 6) In the focus view tab of UCP, type in the X and Y coordinates as (x=53mm, y=51mm). Once we have finished typing in the coordinates pressed the GO button in red and the red pointer moved to the expected location.
- 7) Launched Adobe Illustrator CS6, and opened the designing file “Reaction pad (μ PAD_V_4)_8_17_2015.ai” (can be updated by latest version depended on different purposes) for laser cutting with the power: 90% and speed: 100%. The thickness setting was 0.5mm. In the material database tab of the UCP, chose nature>paper>nitrocellulose paper.

BioDot Protocol

- 1) Prepared PBS with 1mg/mL bovine serum albumin (BSA), 0.05% SDS and 2% Ethanol in the 96-well plate. The wells, A1~A5 and B1~B4, hold 200 μ L of the mixed reagents. Once we have prepared the reagents, we placed the well plate on the BioDot system waiting for the dispensing.

- 2) Placed three nitrocellulose membrane card with different flow rate, HF75, HF135, and HF180, which have already been cut by laser cutter onto the nest. We lined up the long edge of these materials to the right edge of the nest. Then switched on the vacuum for fixing the materials on the nest.
- 3) We opened the scripts with 2*50nL protocol and ran the BioDot aspirating/dispensing system twice on the same protocol.
- 4) After the materials have been done the protocol with BioDot, we took them out and dried them at room temperature for 2 hours.

Staining Protocol

- 1) We placed the materials in a box and rinsed off them with ddH₂O.
- 2) Added enough Ponceau S to cover the materials and rocked it until we can see the signals of stained protein (T=3min).
- 3) Discard the Ponceau S and rinsed with ddH₂O; rinsed and discarded repeatedly until the pink stops bleeding strongly.
- 4) We washed off the materials with ddH₂O in 5min increments until the materials were completely cleaned off.
- 5) Imaged the results using a flatbed scanner or camera.

2.2.5. Integrated Assays

Dose-response Experiment

Materials Preparation

- 1) There are four components of the LFIA strip. For the hydrophobic pad, we printed it out on the wax printer and heated it in the oven for 3min at 250°C.

- 2) We opened the designing files (Adobe Illustrator) and repeated the Cutting Protocol showed above, included the absorbent pad, wax-treated hydrophobic pad, reaction pad (we used H180 in this experiment) and sample pad.

Reagents Preparation

- 1) We prepared 200 μ L of capturing reagents at 0.1mg/mL final concentration for spotting. The reagents contained six antibodies for different pathogens, they are anti-Norovirus GII.4 Ab, anti-Norovirus GI Ab, Rotavirus Ab, anti-PBP-2a Ab, anti-Giardia Ab and Anti- Cryptosporidium; and one more antibody, Goat anti-mouse Ab.
- 2) Repeated the BioDot Protocol showed above. Then we dried the HF180 at room temperature for 48 hours.
- 3) Once HF180 cards dried out completely, we placed them into a box which contained 1% BSA reagents to block the membrane surface for avoiding non-specific binding for 30min.
- 4) Prepared sample, mixed PBS, Tween 20, AuNp, Anti-Norovirus Ab (stock concentration 0.75mg/ml) and Norovirus GII.4 VLPs (stock concentration 1.35mg/mL) in total volume of 100 μ L.

Integration of Cartridge

- 1) Assembled all the components of the LFIA strip together.
- 2) We used the swab to collect the sample incubated for 30min already, included the variable concentration of Norovirus GII.4 VLPs (0 pM to 1000pM), PBS, AuNps, anti-Norovirus Ab and tween 20, from the 1mL tube. Following collection, the swab was inserted into the first chamber of the *ParatusSDS*[®]

Cartridge. Then we closed the lid and pressed the button-like plunger which pushed 200 μ L buffer through the holding chamber. After that, the sample extracted from the swab to the second chamber and then introduced on our strip.

Gold Enhancement Reactions

- 1) We dispensed Solution A of the gold enhancement solution in the 1mL tube and then added solution B. Mix them thoroughly and waited for 5min.
- 2) We added solution C and Solution D and mixed completely.
- 3) Then we pipetted 100 μ L to cover the reaction area presented signals of the LFIA strip for incubating 10min.
- 4) Imaged the results after gold enhancement using a flatbed scanner or camera.

2.3. Results and Discussions

2.3.1. Optimization of Spotting Parameters and Material Flow Rate

Initially, we used a bovine serum albumin (BSA) protein solution (1mg/ml in PBS) as the spotting solution to optimize the instrument parameters and software scripts for array printing onto the prototype LFIA strips, including x- and y- coordinate offsets between each spot within the array and between each LFIA strip to center the array within the 7mm nitrocellulose channel width. Figure 6 shows a nitrocellulose membrane card, laser cut and spotted with the optimized spatial patterning protocol. Based upon visual inspection, a high degree of consistency and reproducibility was found among the individual LFIA strips using a pitch of 1.5 mm between each spot and 15mm offset distance between each strip.

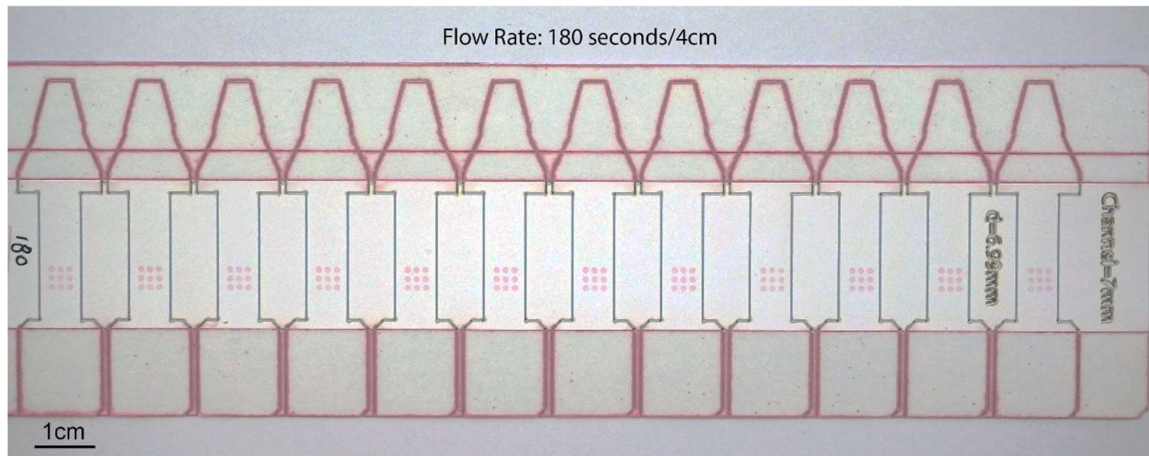


Figure 6. Example nitrocellulose strip printed with 2-50 nL BSA and stained using Panceau S. Dispensing protocols were deemed to be optimal when discrete, non-overlapping spots were present and the arrays were roughly centered within each LFIA strip reaction area. Picture brightness/contrast enhanced for printing and visualization purposes only.

Next, different nitrocellulose materials were examined to determine which material would best support the desired deposition volume (2-50 nL droplets) in a 3 x 3 pattern within the 7mm width nitrocellulose strip, as flow (i.e. wicking) rates affect the minimum or maximum spot-spot separation and volume. As shown in Figure 7, BSA protein printed onto different nitrocellulose materials generated overlapping and non-

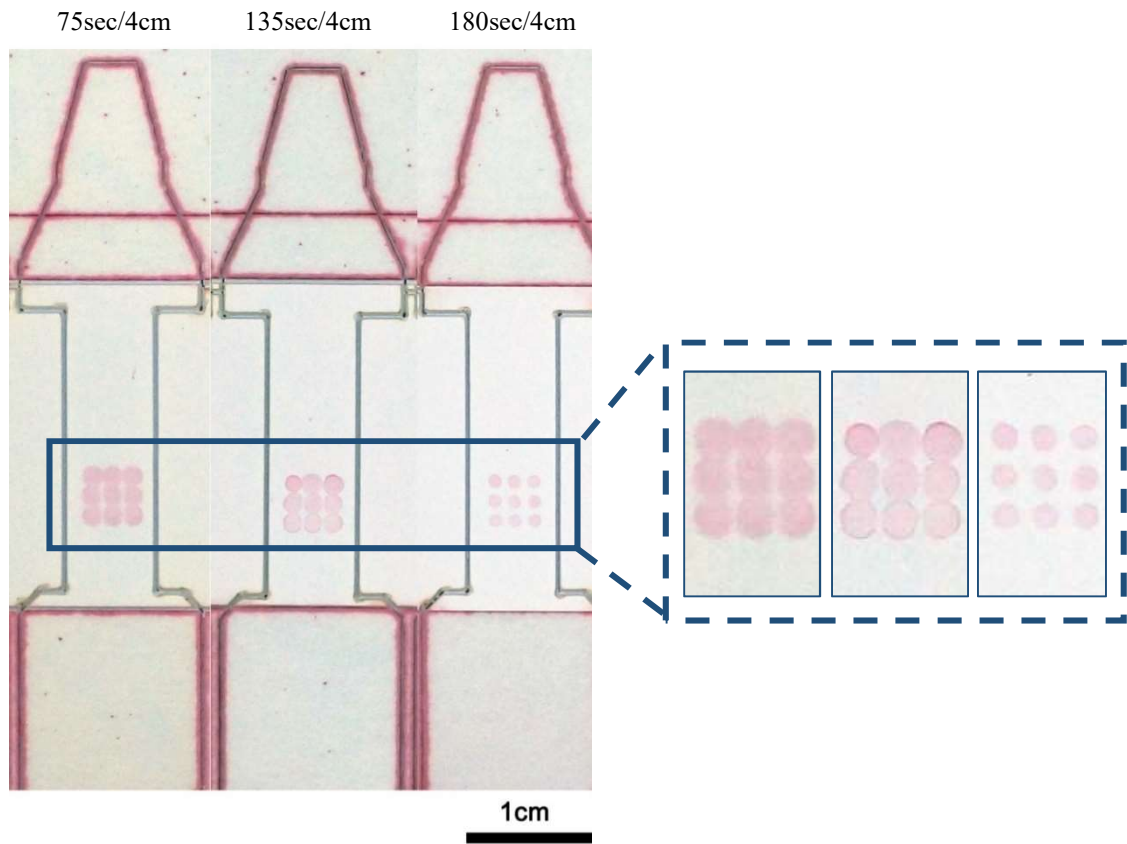


Figure 7. Effect of nitrocellulose material and flow rate on array patterning.

discrete array spots in both the HF75 and HF135 materials with a flow rate of 75sec./4cm and 135sec./4cm, respectively. In comparison, the HF180 material (flow rate 180sec/4cm) demonstrated discrete, well-resolved array spots with clear edges such that each of the dots could be recognized visibly without any overlap (Figure 7). The spot sizes were measured using digital calipers and plotted in Figure 8, revealing a mean spot

size of 1.84mm, 1.72 mm, and 1.2 mm for HF75, HF135, and HF180 materials, respectively. As expected, the highest porosity, slowest flow rate material (HF180) exhibited the smallest spot size when following the 2-50 nL BSA in PBS deposition protocol. Subsequent addition of 10-20% ethanol into the capture buffer improved spot resolution of 2-50 nL droplets even in the HF75 material (data not shown).

2.3.2. Norovirus Detection in LFIA Strips

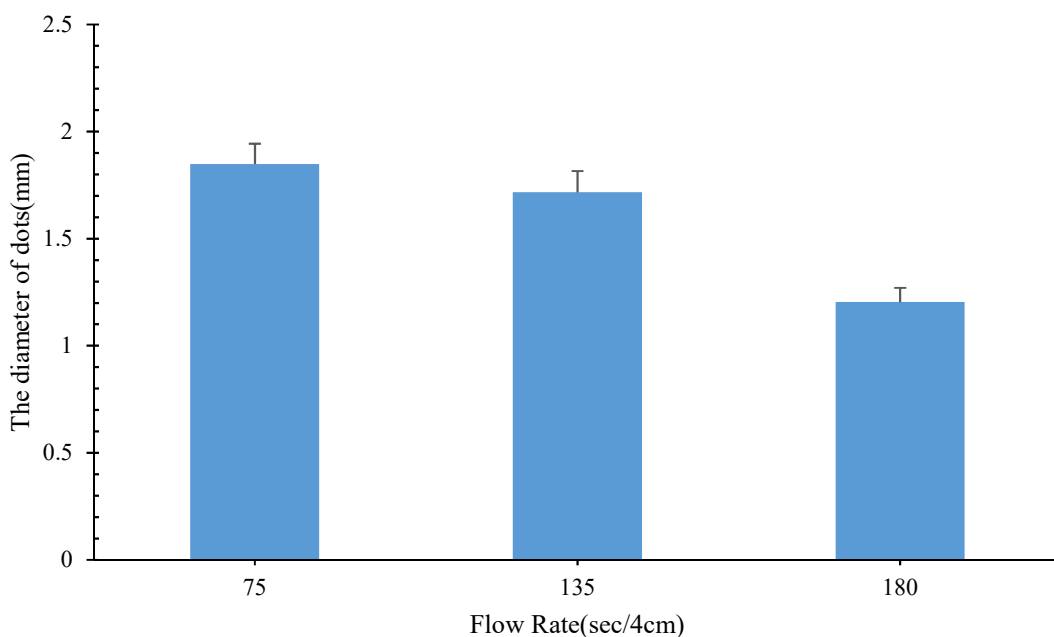


Figure 8. Measured spot diameters in various nitrocellulose materials.

We examined the impact of the nitrocellulose materials and their respective flow rates on an existing sandwich-based immunoassay developed in the Weigum lab, for detection of Norovirus GII.4, which is the major cause of food-borne GE in the United States. We printed the arrays as described above and introduced a pre-mixed sample spiked with Norovirus GII.4 VLPs and AuNPs-coated with detecting antibodies onto the LFIA sample pads for colorimetric detection of Norovirus at the lower left array spot (Figure 5). The results are shown in Figure 9 and reveal that the HF180 material

(180sec/4cm) had the highest signal intensity and signal-to-background ratio in the presence of Norovirus VLPs. In comparison, the HF 75 material (75sec/4cm) generated

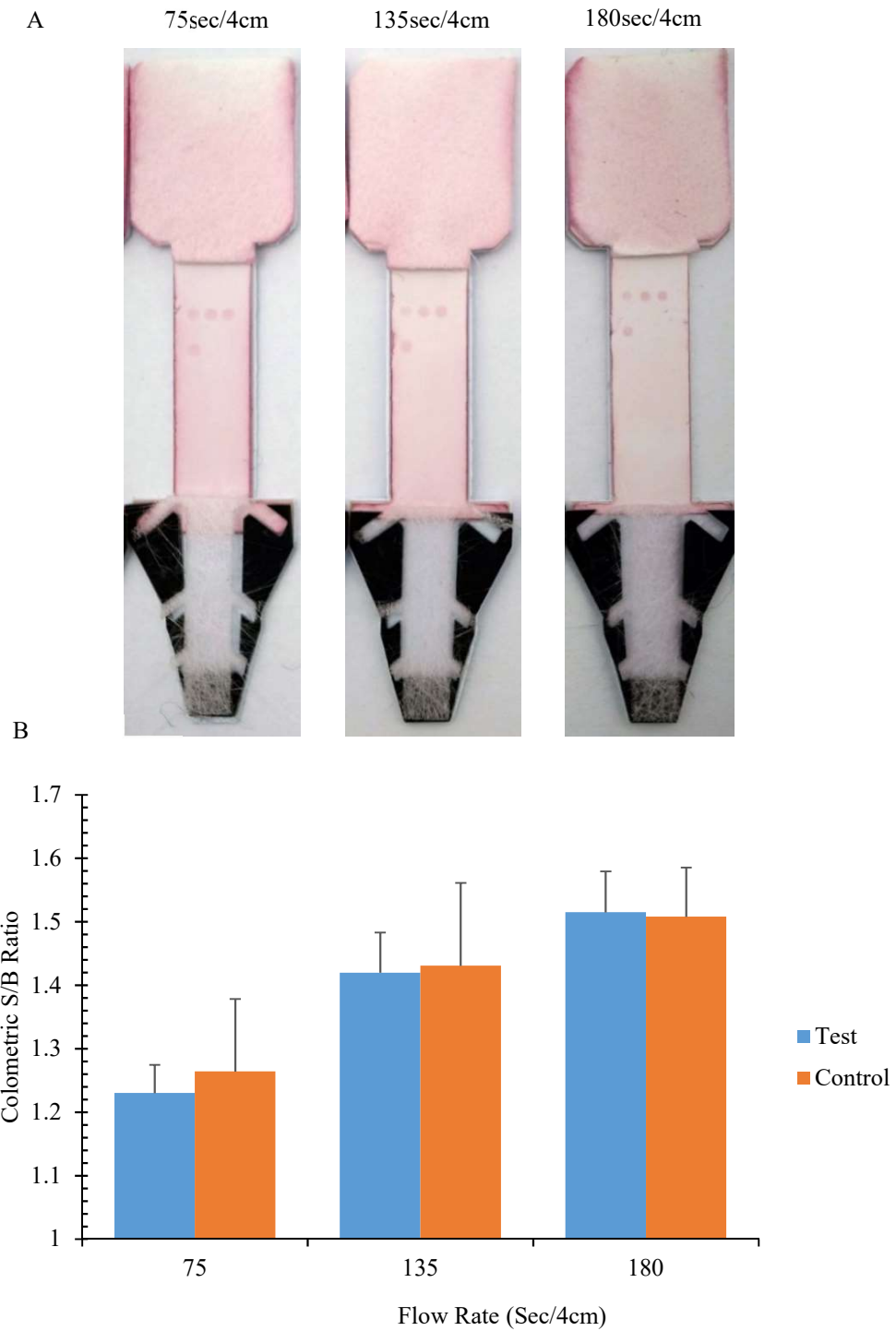


Figure 9. Comparison the signal intensity among 75sec/4cm, 135sec/4cm and 180sec/4cm. Upper figure shows the device after the test, there are Norovirus positive signal on them. The bottom is the plots based on the upper figure quantized by the ImageJ.

the lowest signal intensity and the signal-to-background ratio (Figure 9 B). These results can be easily understood by the fact that the faster flow rate materials provide less time for the capture antibodies to interact with the sample as it quickly flows over the reaction area, versus the slower flow rate materials which provide greater interaction time and, therefore, greater probability of forming a successful sandwich immunocomplex. As such, the HF180 material was selected for all further studies.

2.3.3. Combination of *ParatusSDS*[®] Cartridge and Norovirus LFIA assay

Following the design of the LFIA strips and optimization of the array spotting protocols, we aimed to integrate the two-stage *ParatusSDS*[®] Cartridge with the Norovirus LFIA test demonstrating combined sample preparation and detection. Array patterning was performed as described above using the panel of 6 diarrhea-related pathogens or toxins (Figure 3); however, for simplicity, only one of the target pathogens (Norovirus GII.4) was present in the mock sample introduced into the *ParatusSDS*[®] Cartridge. The overall assay sequence involved spiking a buffer solution with a known concentration of Norovirus GII.4 virus-like particles (VLPs), adding the anti-Norovirus coated gold nanoparticles (detecting antibody/colorimetric reporter), mixing for 30min., then collecting this sample (~100µL) onto a small flocked swab (*FLOQSwab*[™] Copan Diagnostics, Inc. Murrieta, CA) (Figure 6). The swab was then placed into the first chamber of the *ParatusSDS*[®] Cartridge, the lid was closed and sealed. The sample was eluted from the swab by pressing the first actuation “button” which triggers a 200µL volume of elution buffer into the first chamber specially designed to maximize turbulent mixing/extraction of the sample from the swab flowing into the second chamber. The inserted LFIA strip sample inlet came into contact with the eluted sample within the

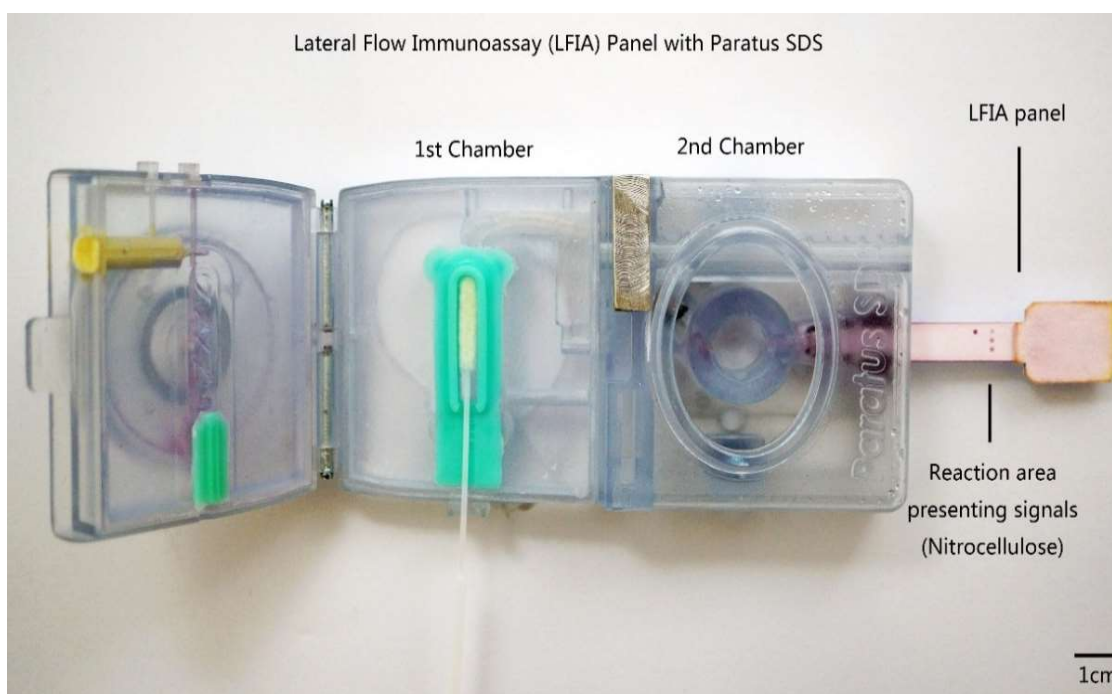
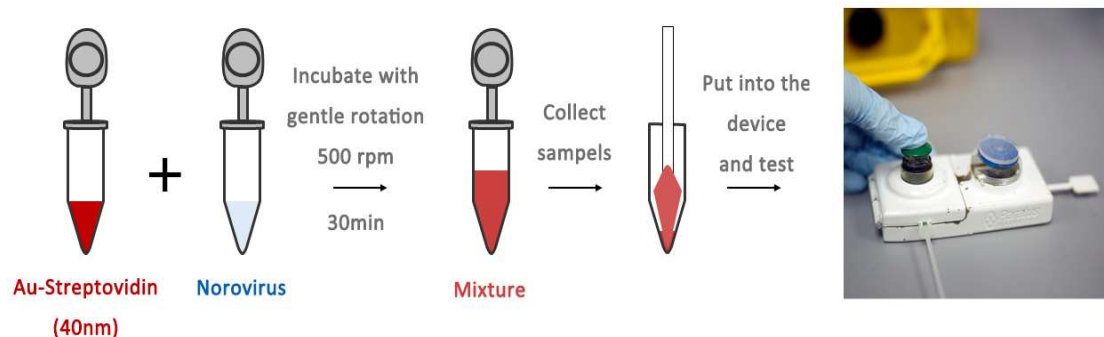


Figure 10. Integrated LFIA assay for Norovirus with the *ParatusSDS*[®] Cartridge. In the final test strip, there were four positive array spots within reaction area; three controls, located in the right column closest to the absorbent pad, indicate that the LFIA test functioned properly to form sandwich immunocomplexes, while the left column, top spot is the only target-specific array spot with a positive reaction indicating the presence of Norovirus antigen within the sample.

second chamber and began wicking fluid into the LFIA strip (Figure 10). A successful LFIA test was visible of a pink/red color that developed at the three built-in control spots within the array, while a Norovirus GII.4 positive test was visible of a pink/red color that developed exclusively at the anti-NV GII.4 capture site (Figure 10).

Next, a dose-response series tested the lower limit-of-detection for the integrated assay using a range of Norovirus VLPs between 0 – 1 nM, spiked into the buffer. These

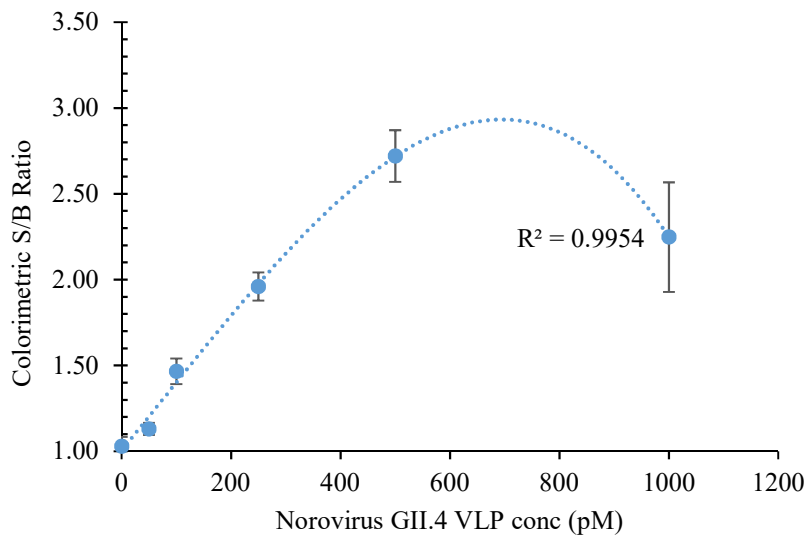
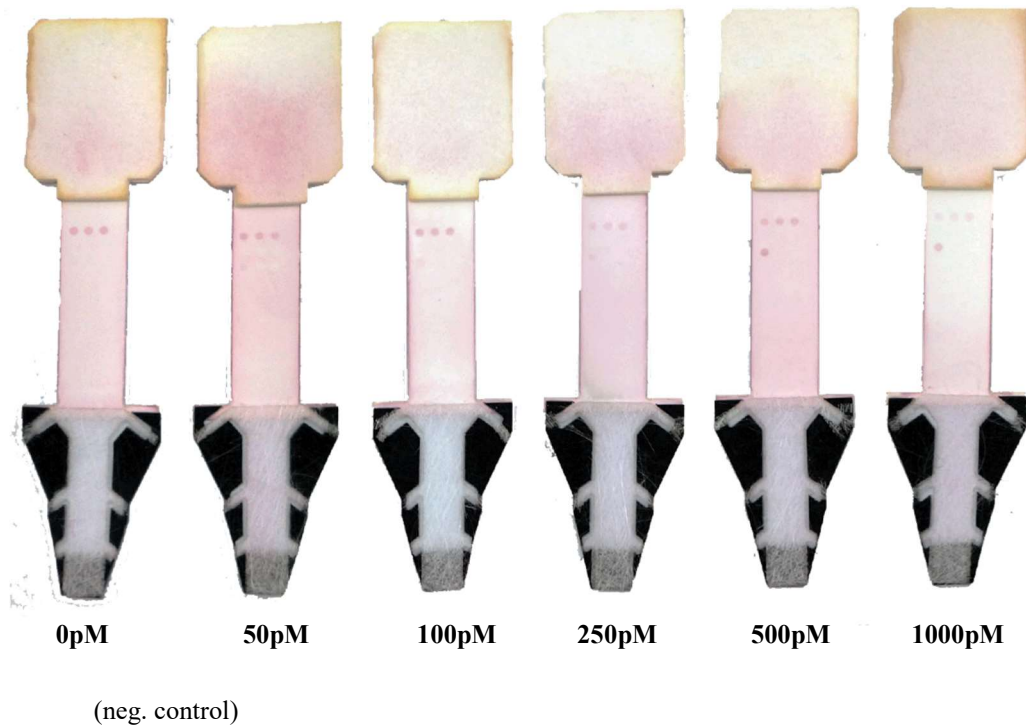


Figure 11. Dose-response data and curve for integrated μ PAD Norovirus assays with Paratus SDS® Cartridge. Data collected and figure assembled with the assistance of K. Ranjan.

experiments were performed in collaboration with another graduate student in the Weigum Lab, Kshitij Ranjan. Figure 12 shows that the positive NV signal was visible in samples containing at least 50 pM VLPs and that those containing less than 50 pM VLPs were negative. Quantitative pixel analysis in Image J using hand-selected regions of

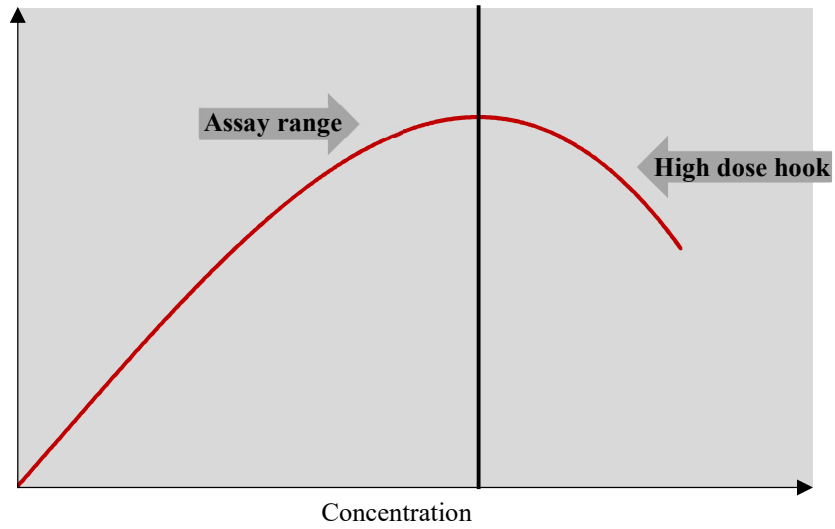


Figure 12. A high dose hook is observed in the plotted curve when high antigen concentration has been introduced into an immunoassay test.

interest (ROI) that encompassed the NV spot area minus the background further revealed a dose-response range below 500 pM (Figure 11). These studies are currently being repeated in order to establish a true analytical sensitivity with appropriate standard deviations to estimate inter- and intra-assay variation.

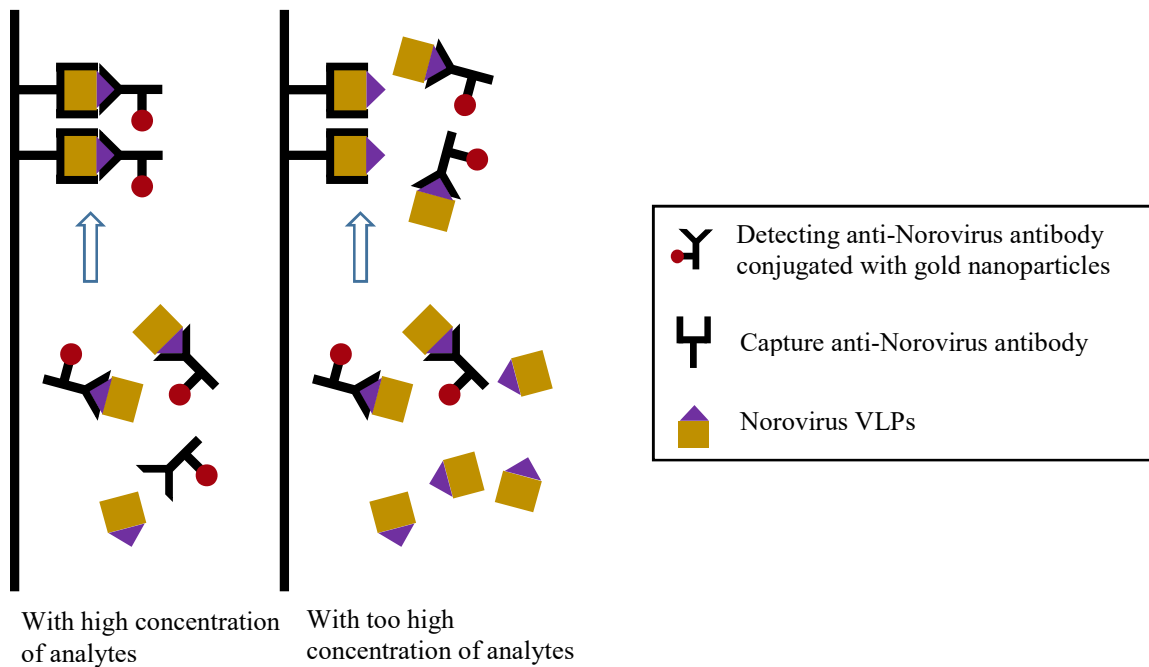


Figure 13. High dose hook effect.

As the plot shows, the signal intensity decreased at the concentration of 1000pM. As we expected, 1000pM concentration should have the highest signal intensity, however, the plot shows the opposite result. Under a condition, we do not change the concentration of antibodies or other variation. When we have a very high concentration of analytes in our sample which may cause that there are not enough detecting Ab to recognize with the excess antigen; and after introducing sample onto the reaction area the capture Ab will bind with that excess antigen, which will prevent the mobile Ab-Antigen complex from binding. And after washing, the signal will be weak or even become negative. Thus, this is called hook effect (Figure 12, 13).

The relatively faint signals generated from the AuNP detecting particles (40 nm diameter) used in these preliminary experiments confirmed the need for additional strategies to amplify the signal and increase contrast. To this end, we explored a simple

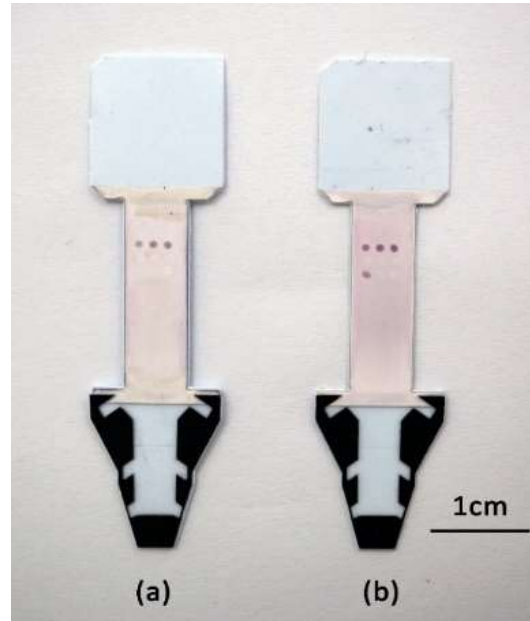


Figure 14. (a) Control group (left, with 0 pM norovirus) shows three dots (incubated by Goat anti-mouse antibody) on the first line (b) Testing group (right) presents a positive signal of norovirus on the second line left dot incubated by 500 pM noroviruses.

catalytic reaction that deposits gold ions, Au(I)^+ or Au(III)^+ , in solution onto the surface of gold nanoparticles in the presence of a reducing agent forming metallic gold (Bailey *et al.*, 1999; Hainfeld & Powell, 2002). This process, known as auto metallography, induces a nucleation effect that increases the size of the AuNPs, thereby altering the AuNP light absorption and scattering properties to yield a high contrast, black/blue colorimetric signal. Norovirus LFIA strips incubated with the GoldEnhance™ reagents following the LFIA test in the presence of 500 pM NV-VLPs demonstrated a strong color reaction that could clearly be distinguished from the background at the NV capture array spot along

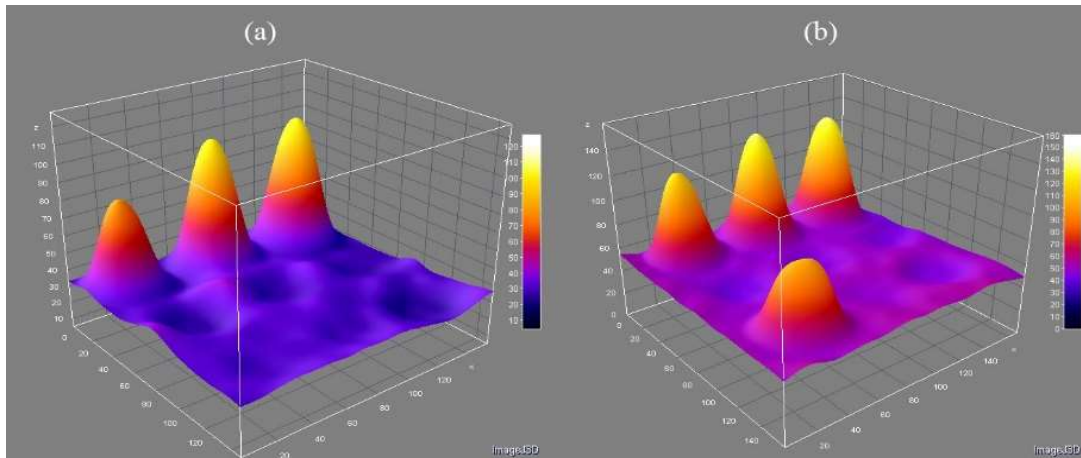


Figure 15. The height of the peak presents the intensity of signals showed on the surface of membrane. with the positive control areas (Figure 14). To quantify the result in Figure 14, we used ImageJ and made a surface plot (Figure 15). The height of the peak presents the intensity of signals showed on the surface of the membrane. Left channel is the control group presented three dots of GAM with a high peak in orange/yellow; right channel is the test group; rear line presents Norovirus-positive with a high peak in orange/yellow (Figure 15). Also, we compared it with the one without gold enhancement. It appears that the one treated by gold enhancement has a stronger signal (Figure 16).

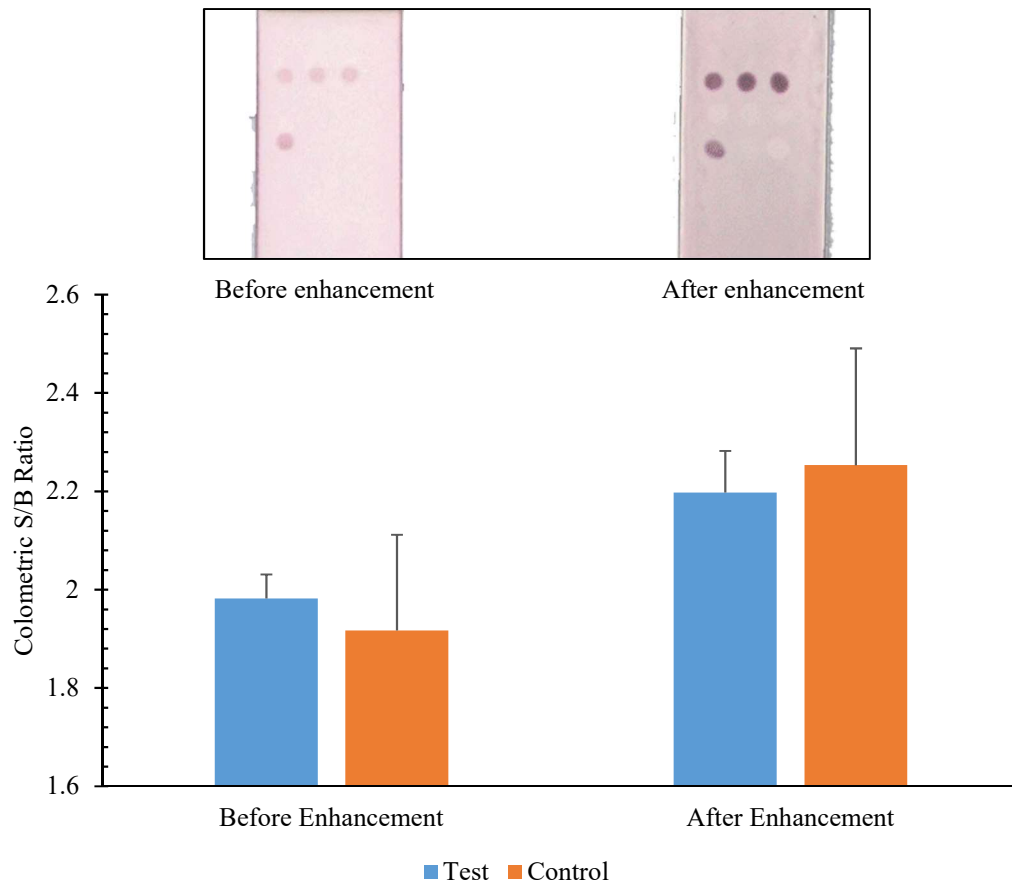


Figure 16. The signal intensity comparison between the group before gold enhancement treated and after gold enhancement. Right one is treated by the gold enhancement showing a stronger signal intensity with dark purple color. Also, the plot presents the same result.

3. DESIGN FULLY INTEGRATED LFIA STRUCTURE WITH SECOND-GENERATION *ParatusSDS*[®] CARTRIDGE

3.1. Timed Delivery - Network Design for Multistep Assays

3.1.1. 2-Dimension Geometry-Based Programmable Network

We have redesigned our LFIA panel to the footprint of *ParatusSDS*[®] Cartridge and set up our panel into it as an integration device with a timed delivery function.

Since multiple steps (e.g., target binding with capture antibodies, washing and amplified signal development) (B. Lutz *et al.*, 2013) were involved the processing of detection on our LFIA, it was essential to configure the LFIA network to accommodate

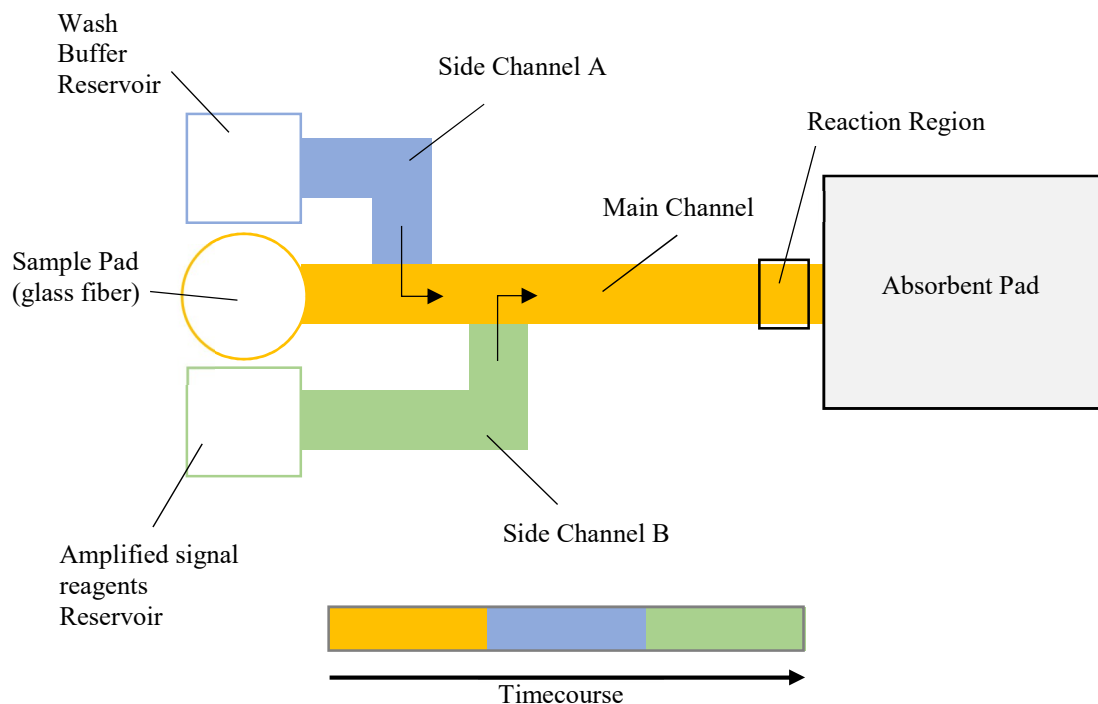


Figure 17. Basic network of Multistep paper-based assay panel. The sample solution collected by the sample Pad will reach the reaction region through the main channel at first (orange), and then the buffer(blue) washes off the extra reagents from the reaction area; lastly, the amplified solution from the reservoir(green) will get into the main channel via the side channel.

multiple inlets for each reagent, with timed delivery of reagents in sequence to the

reaction/detection zone (Toley *et al.*, 2013). We created variable length arms to delay the time for washing buffer and amplified signal solution entering the main channel. This timing delivery structure with variable length arms was designed to allow enough time for capture antibodies to recognize and bind with the pathogens in the sample solution before the other two reagents merge into the main channel one after the other (Figure 17).

However, while we were doing the preliminary test using food dye in this three-inlet network, there was a backflow issue where the main channel reagent (sample) flowed into the side channels. (Figure 18). This issue is illustrated in Figure 18 using a

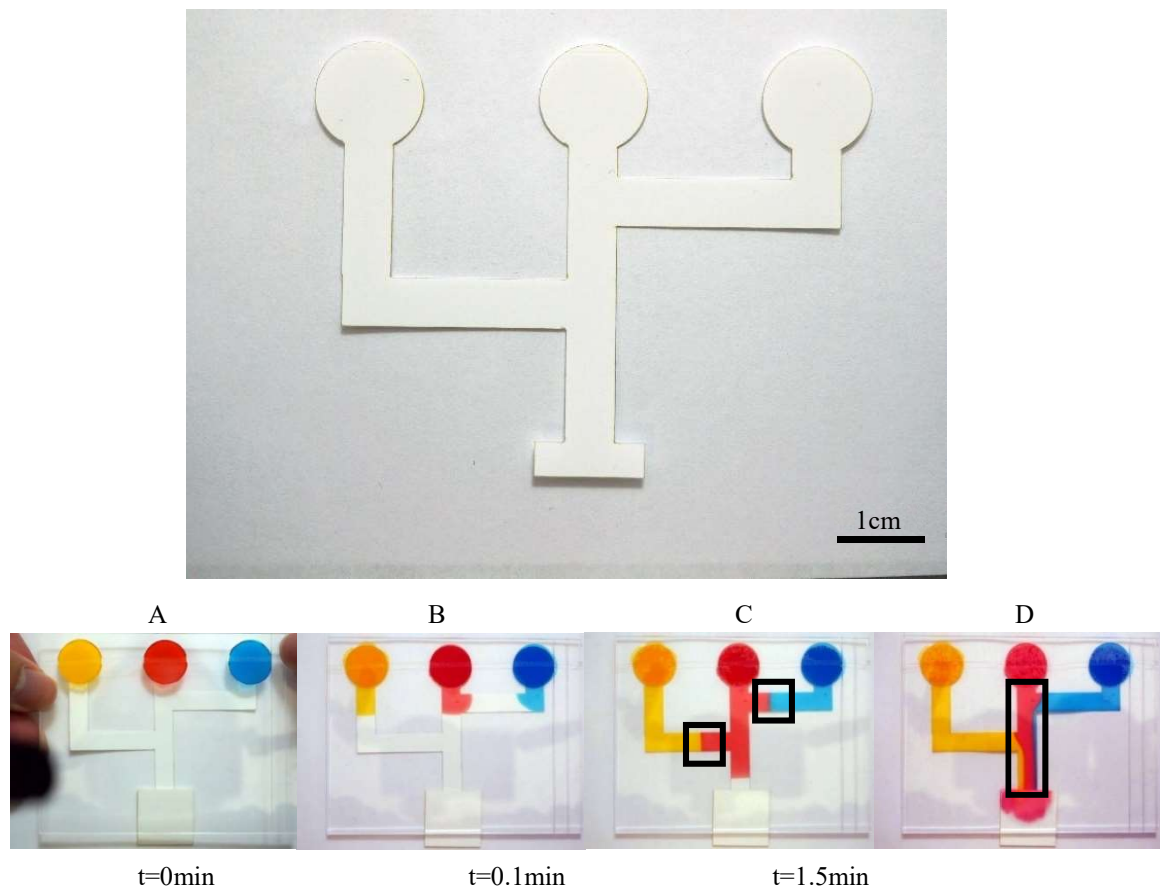


Figure 18. The upper is the prototype version of three inlets structure. Three circular inlets for introducing sample fluidic, then the fluid will flow through into the channels and reach the reaction area. The bottom is the time line of the laminar flow test. (A) For decreasing the variation and avoid the error on different introducing time, we adhered three piece of glass fiber to the acrylic panel and then pipetted three different food dye of 300 μ L each onto the glass fiber. Then we aligned the acrylic panel up to the network. (B)(C)(D) Three food dye got into the nitrocellulose membrane by the capillary force and then wicked by the absorbent pad.

modified structure containing three circular inlets, two side channels, one main channel and one joint for connecting with the absorbent pad by a laser cutter. The red food dye in the main channel passed through and flowed into the both side channel where the blue and red food dye was moving through (Figure 18 C) and only after meeting the fluid boundary of the blue/yellow dyes was the red dye pushed back toward the main channel. The other problem illustrated in this Figure 18 D, was not entirely unexpected and was a nice demonstration of laminar flow in microfluidic devices. When laminar flow occurs, the only mixing of reagents is at the diffusion boundary between fluids (Batchelor, 2000; Geankoplis, 2003). In the lateral flow immunoassay, all the reagents needed to react with the embedded capture reagents at the reaction area evenly, which was not possible due to this laminar flow phenomenon. Moreover, the footprint, or usable space, for our LFIA strip in the prototype *ParatusSDS*[®] *Cartridge* was limited due to the room for a swab and other structures. Therefore, the first step for re-design was to avoid any fluids entering into the side channel from the main channel and reduced the size of itself.

We designed an inline network with three inlets lined up in series with the main

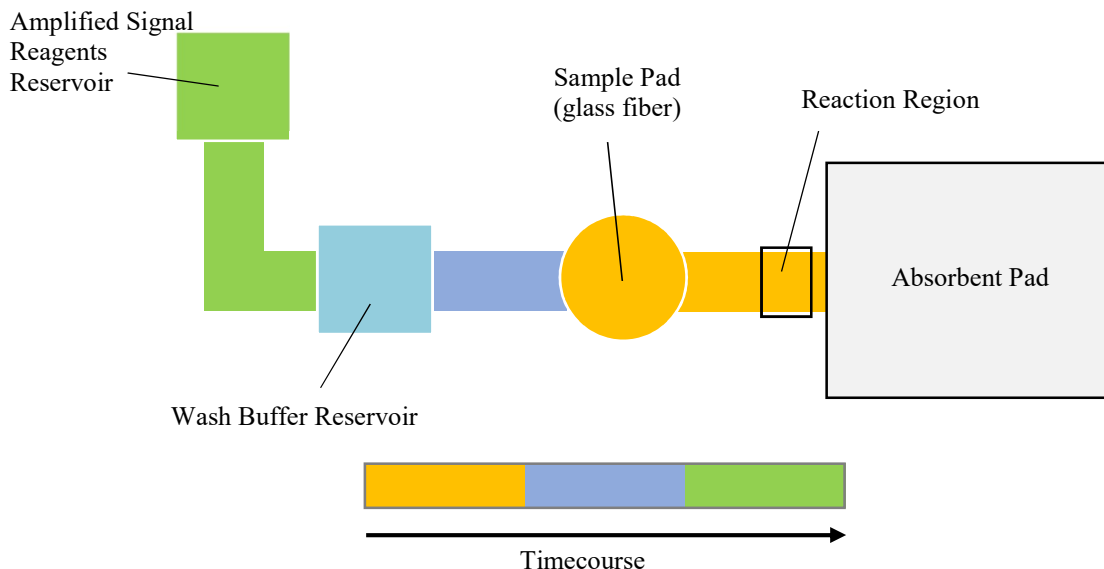


Figure 19. Inline network test. Three inlets will introduce sample, wash buffer and amplified signal reagents. These three fluid should reach the reaction region by order and without any mixing with other two reagents. At the end, the excess reagents will be wicked by the absorbent pad.

channel covered by three circular glass fiber for holding and introducing fluid into nitrocellulose membrane (Figure 19, 20). Even fluids introduced from the former two glass fiber caused backflow moving backward to the next glass fiber, the flow afterward pushed the back-flows forward to the absorbent pad due to the laminar flow (Figure 20 B, C). In Figure 20, we pipetted three different food dye: yellow, blue and red treated as a

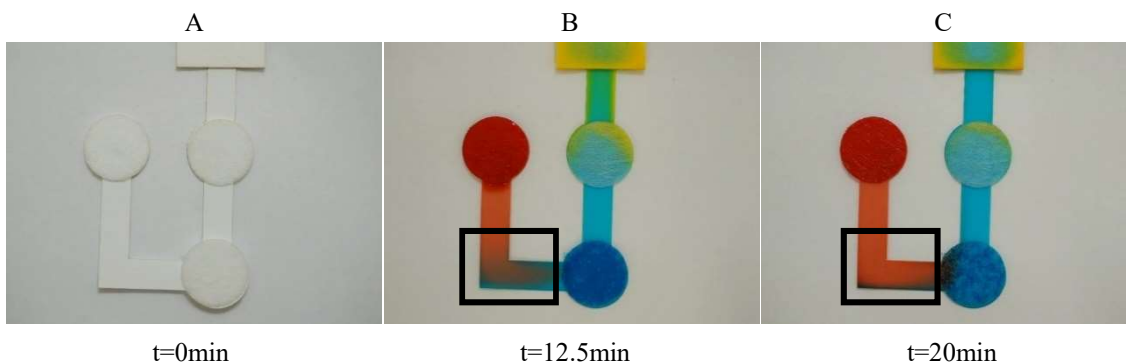


Figure 20. Inline network test. (a) The combination of the micro device includes three circular glass fiber, nitrocellulose membrane and absorbent pad. All these components have been fabricated by laser cutter. (b) and (c) shows the red food dye push the blue food dye forward to the absorbent pad, meanwhile the blue dye is pushing the yellow dye to the sink also with a little diffusion.

sample, wash buffer and amplified reagents, respectively. When the backflow of blue dye was flowing backward and met the red dye, the blue dye stopped moving backward and then was pushing by the red dye. Due to the elimination of side channel, the size of the network has been decreased significantly. Thereby, for now, the design of inline-based network matches our goal for the integration of *ParatusSDS*[®] Cartridge and our network.

The second purpose of this configuration of the network was to design a special structure to program different time delay for different reagents to reach the reaction area based on the inline network. Actually, a number of fluidic controlling devices have been demonstrated by others in the microfluidics field. One method is to place an absorbent-based shunt into and contact with the nitrocellulose membrane (Toley *et al.*, 2013). The delay can be controlled by changing the length or thickness of the shunt. The other method is using dissolvable sugar applied to the nitrocellulose membrane to establish multi-step programmable flow delays (B. Lutz *et al.*, 2013). The simplest way is to change the channel geometry as demonstrated by Yager's group who varied the shape of the channel building a sudden-expansion/contraction strip geometries to increase/decrease the time spent on the frontline of fluid moved (Fu *et al.*, 2011). In another case, a serpentine-based structure made from glass fiber replaces the nitrocellulose membrane. Glass fiber plays the role as a conducting channel to introduce the fluid to the main channel (nitrocellulose membrane) (Toley *et al.*, 2015).

To simplify the methods, we applied the two adjustable parameters, length and width, to our network by using the characteristics of two different material, nitrocellulose membrane and glass fiber.

In a porous membrane sheet, e.g. nitrocellulose membrane and glass fiber, the fluid front follows the Washburn equation during the wet-out process (Fu *et al.*, 2011; Washburn, 1921).

$$L^2 = \frac{\gamma D t}{4\mu} \quad (1)$$

Where L is the distance from sample pad to the fluid front, t is the time, D is the membrane pore diameter, γ is the surface tension and μ is the viscosity (Fu *et al.*, 2011; Peek, 1934; Williams, 1981). Therefore, we could characterize the Washburn flow as $L = f(\sqrt{t})$. In the case of strips with constant width and different length, 0mm, 10mm, 20mm, 30mm, 40mm and 50mm fed by a non-limiting fluid as expected, the fluid flows obey the increasing transport time as given by the Washburn equation. Thus, an expansion in the length of a channel can be used to adjust the transport time of the reagent delivered.

To apply this hypothesis to our network, we chose nitrocellulose membrane and glass fiber as our potential materials for fabricating network. In the first experiment, we

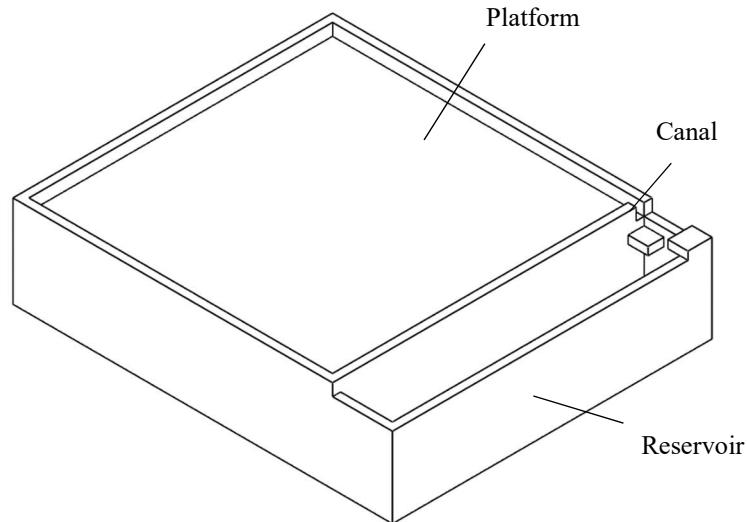


Figure 21. 3D printed device for measuring serpentine structure actuation time. The device made up of three components, platform, canal and reservoir. Platform is for placing timing channel. Canal is for setting up the joint connecting the reservoir and timing channel. Reservoir store the food dye.

only varied the length of the channel. A platform has been designed by Solidworks and

printed out by the 3D printer to place the glass fiber (Figure 21). It consists of platform,

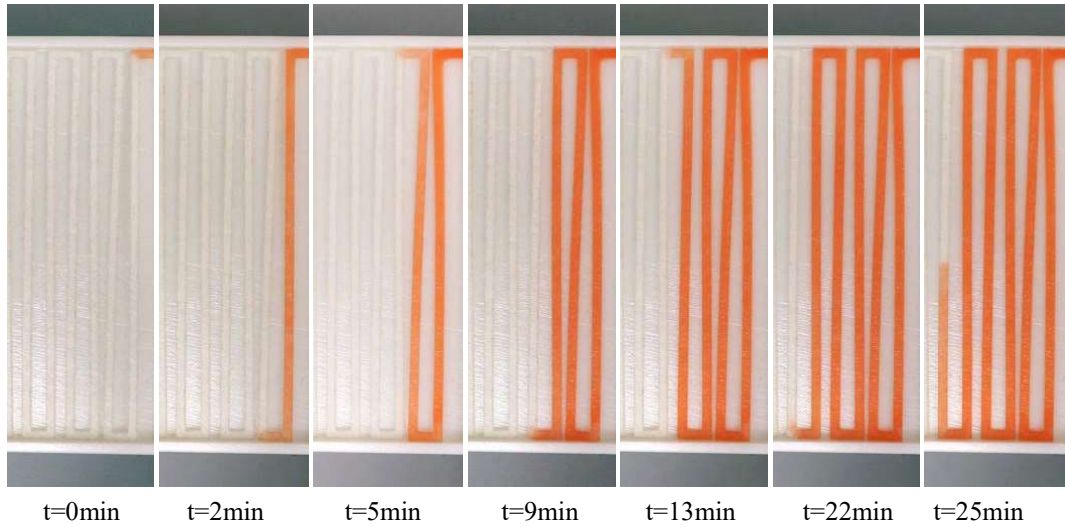


Figure 22. The length-dependent experiment of glass fiber. A series of time-lapse images filmed by the camera. The red food dye has been pre-stored in the reservoir. Then we placed the serpentine-based channel on the platform and introduced the food dye from the reservoir into the glass fiber. The camera started filming at the time, $t=0\text{min}$. After all the dye traversed the channel, we stop the filming.

canal, and reservoir. The canal is for placing the glass fiber channel connected to the reservoir where pre-filled with food dye. Due to the limited space of *ParatusSDS*[®]

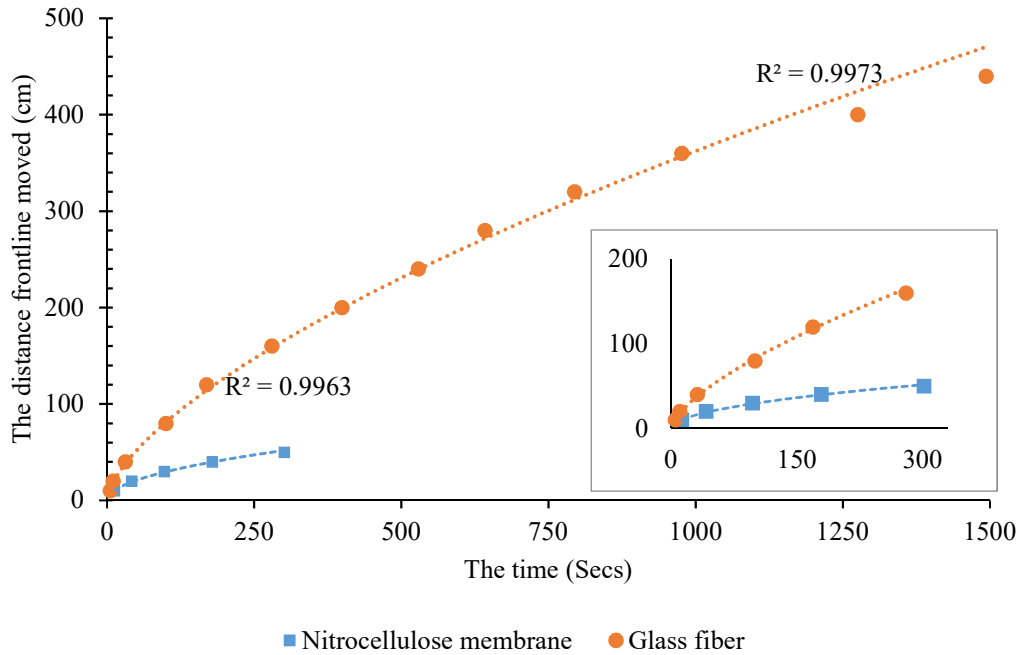


Figure 23. The plot shows length of strips from 0mm to 50mm vs. the time. The orange regression is the experiment based on glass fiber; and the blue one is Nitrocellulose membrane. The plot shows the distance frontline moved is exponential to the root of time which match the Washburn equation, $L^2=f(t)$. In a constant time, the distance frontline moved depends on the pore diameter, $L^2=t*f(D)$.

Cartridge for the network, we designed a serpentine-based structure other than the straight network (Figure 22). The length-dependent experiment based on the glass fiber demonstrated that fits the Washburn equation as the length increasing, the time increasing. The linear plot shows that the distance fluid front line moved was proportional to the root of time as the $L=f(\sqrt{t})$ (Figure 24). Moreover, we also did the experiment based on the nitrocellulose membrane with a smaller pore size than the glass fiber. Comparison between the plots of nitrocellulose membrane and glass fiber present that the results also fit the equation. In a constant time (t), the distance frontline moved

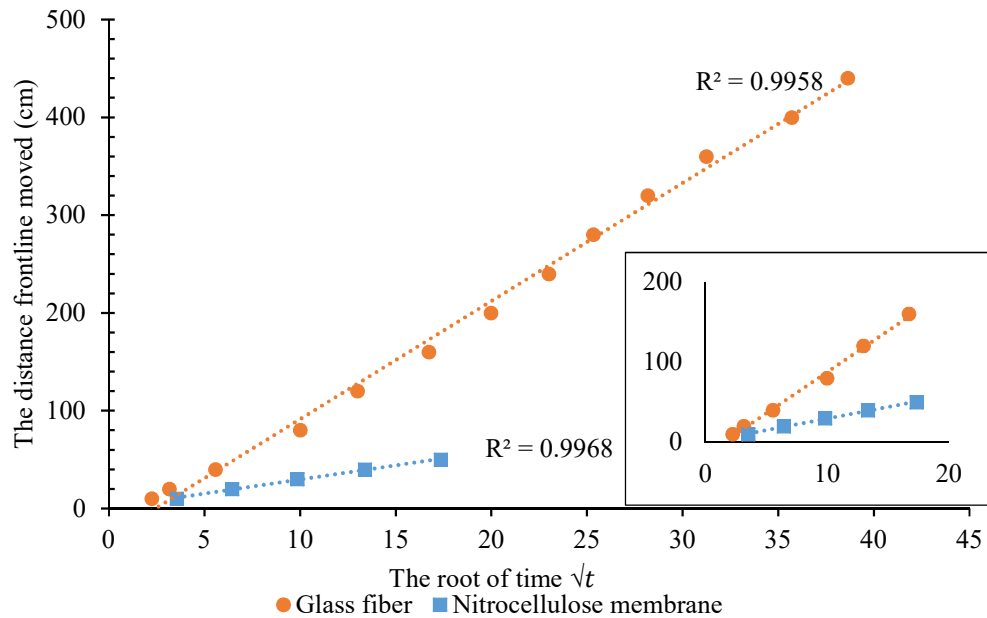


Figure 24. The plot shows length of strips from 0mm to 50mm vs. the square root of time. The orange circle linear is the experiment based on glass fiber; and the blue one is Nitrocellulose membrane. The plot shows the distance frontline moved is proportional to the root of time which match the Washburn equation, $L=f(\sqrt{t})$. In a constant time, the distance frontline moved depends on the pore diameter, $L=\sqrt{t}*f(D)$.

was dependent on the material's pore diameter (Figure 23). The fluid flows faster in a larger pore diameter material than in a smaller one, which means fluid traverses the same distance needed less time in the glass fiber than in the nitrocellulose membrane (Figure 23, 24).

Yager's group also demonstrated a method that changed the channel geometry to achieve sequential delivery of multiple reagents to a reaction area (Fu *et al.*, 2011). They designed a two-cross-section network with a sudden-expansion and sudden-contraction strip geometries. Here, we decided to repeat this experiment to see if it can be applied to our network for establishing a timing channel (Figure 25).

We designed and fabricated two uniform-width channels, one with 2 mm width and the other with 15mm width as the control; and two channels with sudden-expansion parts within the strips (Figure 25). When increasing of width within a strip, in C and B,

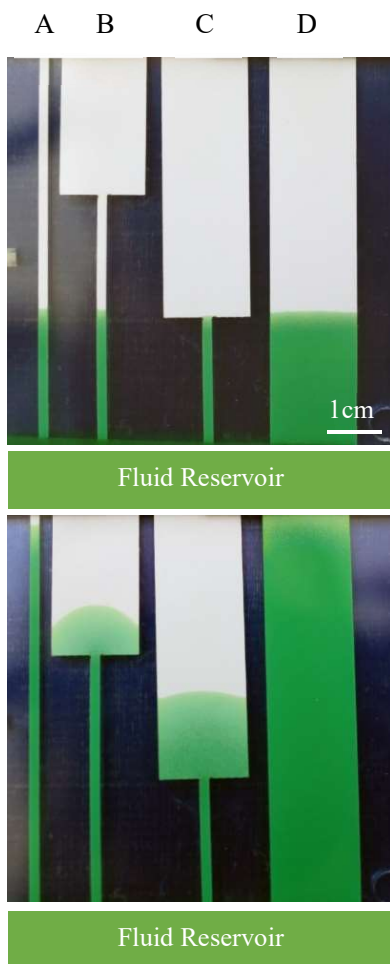


Figure 25. Fluids traverse through into the nitrocellulose membrane during the wet-out process in uniform-width and sudden-expansion channels. The width of A, the first segment of B and C is 2mm; and of D, the second segment of B and C is 15mm.

the Washburn equation is violated. The results actually did not follow the equation. The frontline of fluid flows significantly slower in the process of moving through from a narrow-segment of the strip to the wide segment. We believed this decrease happened in a wider area can be assumed in term of the fluid needed greater time to fill a specific volume element in a length Δy (y is the direction of flow) (Fu *et al.*, 2011) within a wider segment than within the narrower segment. As the data showed (Figure 25), C has the greatest time consuming on the traverse of fluid in a specific Δy , then B, then A and D. As Yager's group demonstrated, the fluid frontline moves slowly in a strip with larger

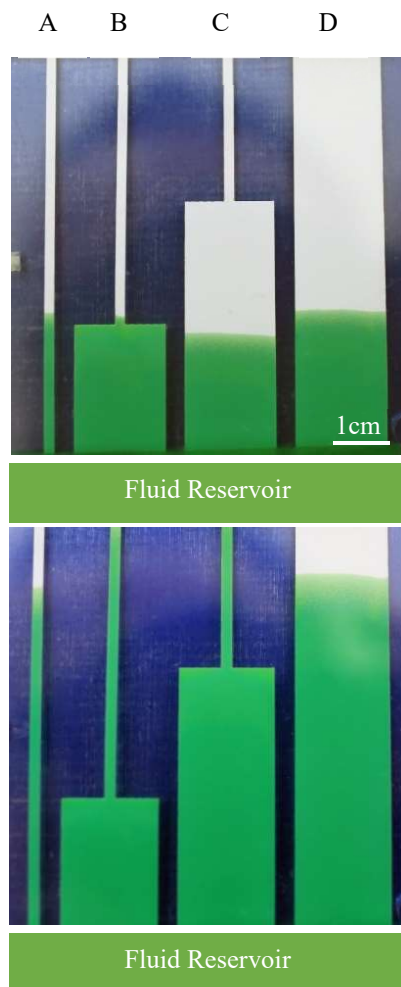


Figure 26. Fluids traverse through into the nitrocellulose membrane during the wet-out process in uniform-width and sudden-contraction channels. The width of A, the second segment of B and C is 2mm; and the width of D, the first segment of B and C is 15mm.

width expansion. Therefore, an expansion of the width of the channel can be used on our network to vary the transport time of different reagents delivered. There are two parameters can be adjusted for transport time, one is the width of the expansion and the other one is the joint location of the downstream (Fu *et al.*, 2011).

In contrast to expansion case, we reversed the inlets of the strip, B, and C, of which the first segment is with a wider width and the second segment with smaller one (Figure 26). The results showed that all the fluids flowing through the first segments consuming the same transport time. However, when the traverse of fluids in the second sudden-contraction segment, the flow of fluid in B was fast, then C and then A and D. This phenomenon can be understood as a smaller area is needed less time for the fluid to fill. Therefore, the sudden-contraction segment in the width of inlets can be used as a tool of decreasing the transport time in our network with a different ratio of two different segments length being an adjustable parameter.

3.1.2. 3-Dimension Geometry-Based Programmable Network

Taking advantage of multi-step procedures of the reagents delivered to achieve high performance on our network, we have demonstrated methods to adjusted 2-dimensions geometry of strip with a variable width of the segment within a single strip and the different length of segments to control timing. At this point, we would like to demonstrate if there is a design also can change the transport time of fluids within the network for multi-step delivery. One previously published method is a design of different length of inlets of vertical nitrocellulose membrane, which were inserted into a fluid reservoir and each of the inlets were disconnected from the reservoir by absorbing different fixed fluid volume (B. R. Lutz *et al.*, 2011). Another lab used surfactant on the microfluidic diodes to build a hydrophobic gap within the flow channel (Chen *et al.*,

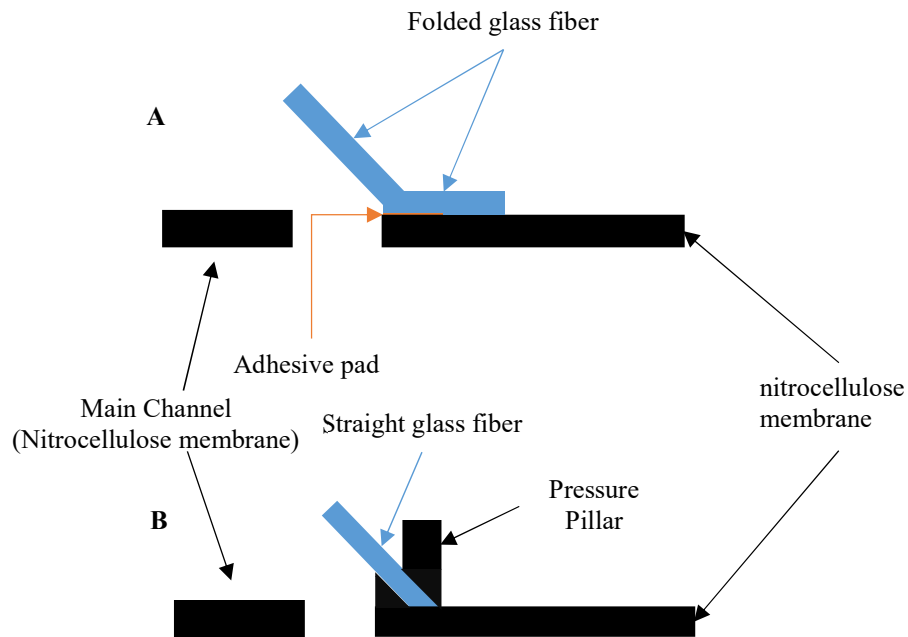


Figure 27. The side view of programmable fluidic driven network. A is using one pre-folded glass fiber as the fluid-triggered moving element placed on the double adhesive pad connected to the nitrocellulose membrane for introducing fluid. B is the one with a straight glass fiber as the fluid-triggered moving element placed underneath of the pressure pillar for fixing the position and on a bottom with a fixed angle; and connected also with nitrocellulose membrane.

2012; Gerbers *et al.*, 2014). Another method is using compressed sponge playing the role as automatic valve actuation for moving the paper strips by wick fixed fluid volume and reach the timing delivery goal based on three expired patent (N. Kurn, 1992; R. A. Bunce & Walker, 1993; R. D. Patel, 1992; Toley *et al.*, 2015).

We have demonstrated a novel method to deliver different reagents in multiple steps using a piece of glass fiber material used as a fluidic triggering element which was placed at a fixed angle relative to the nitrocellulose membrane. This technique utilized gravity to move the trigger down and contact the nitrocellulose membrane initiating flow (Figure 27). The movement of the trigger (cantilever) was based on several parameters which can be described by the following deflection equation (Gere, 2012)

$$\delta_B = \frac{qL^4}{8EI} \quad (2)$$

The elastic deflection of the glass fiber at the free end under a uniform load q (force from fluid gravity per unit length) is given by this equation where L is the length of the glass fiber from the free end to the opposite fixed end; E is the modulus of elasticity; and I is the area moment of inertia of cross section. Which means that the distance the free end moves from the original position down to the final position is based on several parameters: q , L , E and I . Also, I can be given by

$$I = \frac{bh^3}{12} \quad (3)$$

For the rectangular cross section of glass fiber, b is the width of the bending axis and h is the thickness of the bending axis. Since we did not change the material (glass fiber), q , E and h are not variable in our experiments. Thus, the equations (2) and (3) can be simplified to:

$$\delta_B \sim \frac{L^3}{b} \quad (4)$$

This means we can adjust the length and width of the glass fiber to change the deflection.

To demonstrate this experimentally, we cut one piece of glass fiber by laser cutter into a rectangle shape with fixed width and length, then lifted it up into a fixed angle and placed onto and made a contact with the nitrocellulose membrane (Figure 27). After the fluid filled the triggered element, the gravity of the fluid bent the glass fiber allowing the glass fiber to make a contact with the main channel (nitrocellulose membrane, where the detection area located) initiating fluid flow. After that, the capillary force wicked the fluid from glass fiber to the main channel and allowed the fluid to reach the detection area. We had two ways of lifting the glass fiber into a specific angle from the horizontal bottom. One was using a 15g steel weight placed on the folded glass fiber for 48 hours to hold it in a folded status (Figure 27 A). The other one was placing the glass fiber on a sloping bottom with a pressure pillar on the top of it to hold it at a proper location (Figure 27 B).

For a demonstration of these two strategies, we designed two chambers with fluidic reservoirs for mimicking the internal structure of *ParatusSDS*[®] Cartridge (Figure 28). We manufactured these two designs by a 3D printer with 50 μm resolution. Each design consisted of three reservoirs for storing fluid sample and other reagents plus a bottom for placing the glass fiber and the main nitrocellulose membrane channel (Figure 28 A). The glass fiber (bed volume 59μL/cm²) was cut in a rectangle shape. All the fluid triggers were moved down by the fixed fluid volume, e.g., 200μL of food dye. In this experiment, the goal was to demonstrate functionality of the fluid trigger. We pipetted

200 μ L into the reservoir over the fluid trigger. After the glass fiber was wetted out by the fluid and moved down reaching the nitrocellulose membrane, we defined this as one successful actuation process. We did 20 replicates for each method, the failure rate for the group of the pre-folded trigger was 60%, and for the group of the lifting-up-straight

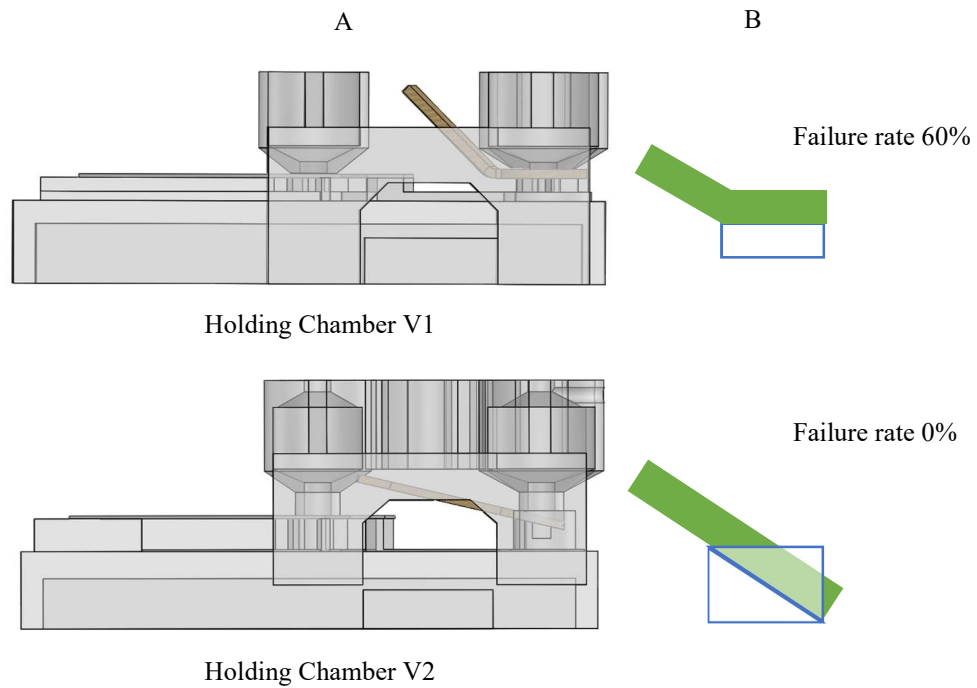


Figure 28. The side view of holding chamber V1 and V2. A channel shows the two versions of holding chamber for different lifting glass fiber methods. B channel shows the failure rate for those fluid triggers do not move down successfully by fixed fluid volume. For pre-folded trigger the failure rate is 61% (n=20), the other one using the slop bottom the failure rate is 0% (n=20).

trigger was 0% (Figure 28 B). As our expectation, the lifting-up-straight trigger moved down to the horizontal line successfully all the time. However, some of the pre-folded triggers did not lay down touching the main channel and still kept at the same angle or some of them just lower down for several degrees from their original angle, even wicked all the food dye we added. Moreover, the other issue was that half of the pre-folded glass fiber returned to the status before folding them into a fixed angle after 48 hours. This phenomenon was not what we expected. Thus, the straight-lifting-up trigger worked

better than the pre-folded. We decided to apply the straight-lifting-up trigger to our multi-step network going forward.

After this, we needed to figure out what were the adjustable parameters that could change the actuation time for the fluidic driven trigger to reach the main channel from the original position. To meet this requirement, we designed a holding chamber with four reservoirs lined up (Figure 29). This device was for measuring different parameters which can adjust the actuation time under consistent settings, e.g. fixed slope angle of the bottom. The width and length of the bottom for placing fluidic driven trigger (FDT) were 7mm and 7mm, respectively.

For the first step of the experiment, we chose to change the width of one segment of the whole FDT. This segment, we named the “neck”, was located right in the first

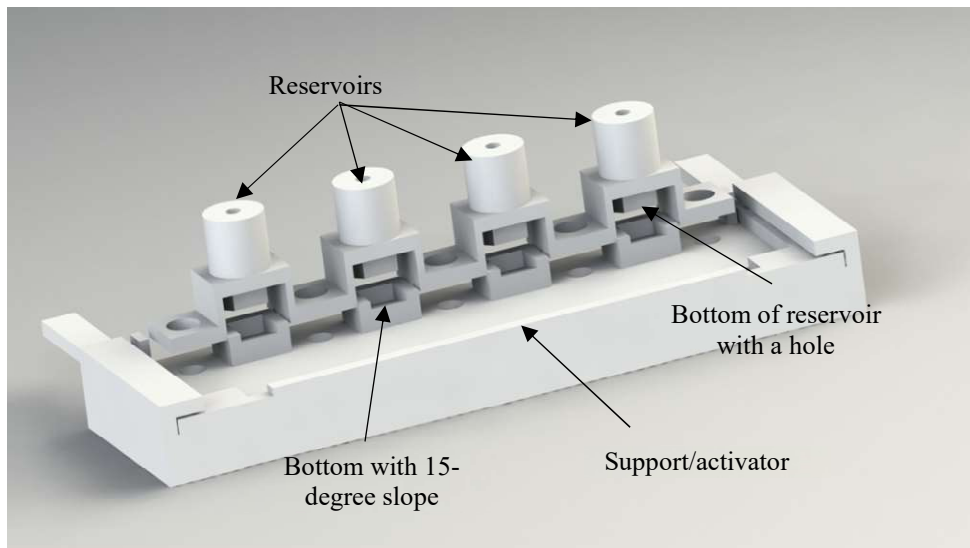


Figure 29. Holding chamber V2.2. Four reservoirs are for reducing the variation and keeping the experiment consistent. The function of the hole on the top of and bottom of the reservoir are for pipetting the fluid and for introducing the fluid out onto the fluidic driven trigger. The bottom (7mm*7mm) for placing the fluidic driven trigger with a 15-degree slope. This slope can make the fluidic driven trigger keep a fixed distance vertically from the support/activator. The whole actuation time is started at the contact between fluid and FDT and ended at the contact between the support and the FDT. Five screws can insert in for tighten and making even pressure on the FDT.

segment placing on the slope bottom of holding chamber. We divided the FDT into two

groups, one group had a neck and the other had no neck. Also, we varied the overall length of both group of FDT with the fixed overall width, which changed the maximum bed volume of fluid, $v=w*l*h$. The gravity of the fluid was also based on the bed volume, $F_g=mg=v\rho g$. Thus, there were two variables in this experiment, the overall length and with/without a neck, one can increase the weight of fluid and one can weaken/strengthen the FDT for keeping itself at a 15-degree angle, respectively. As the result shows, the overall length of FDT was not inversely proportional to the actuation time in the group with the neck (Figure 30), although according to the equation it should be inversely proportional to the actuation time at lengths longer than what was tested (for example lengths >20 cm). In the group w/o neck, the failure rate for the 5cm strips was 100%, which meant all the FDTs failed to contact the nitrocellulose and still stood in the original position. Then for 6cm overall length, failure rate was 75% and for the 7cm length it was 0%, so that all the FDT with 7cm long moved down. Additionally, the actuation time for the group w/o neck with 6cm overall length was greater than that for 7cm overall length. These demonstrated the overall length can change the actuation time of FDT.

Comparison between the group with neck and without a neck, FDT with neck took less time to get down completely. Therefore, the neck structure could be added into

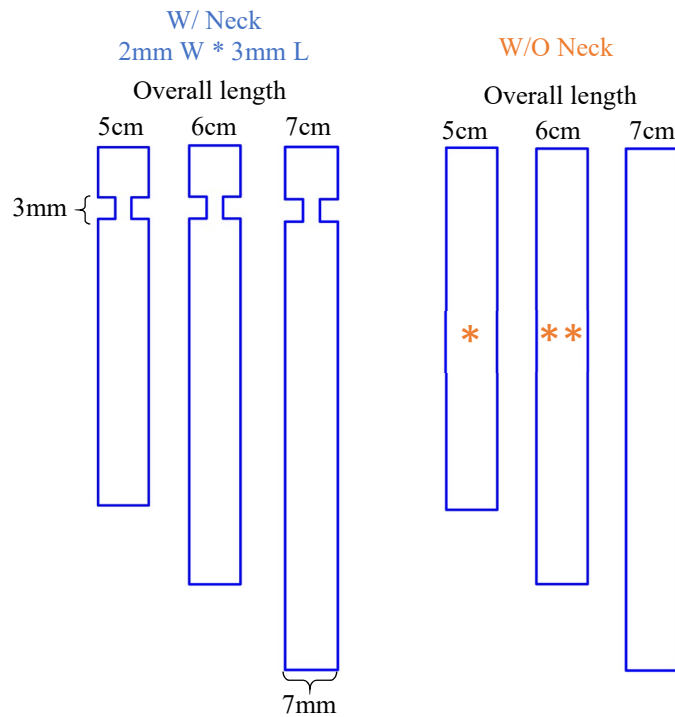
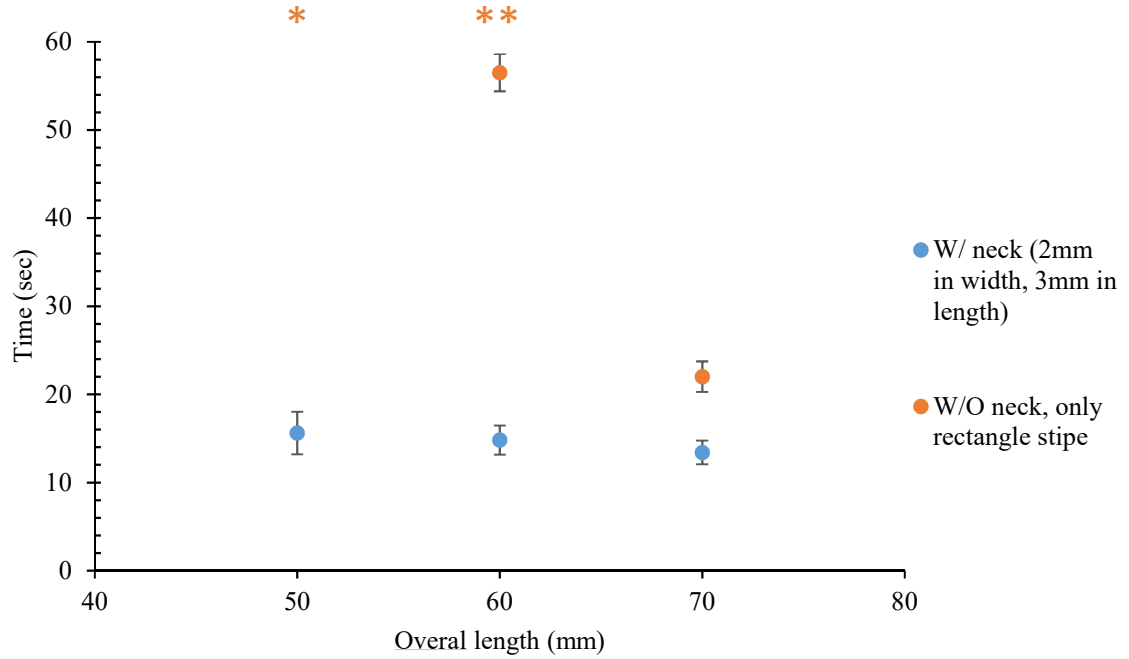


Figure 30. The actuation time of two groups of FDT. One group of FDT is with neck 2mm*3mm and vary the overall length; and the other is without neck and vary the overall length. * 100% failure rate (8 out of 8 trails), none of them can move down. **75% failure rate (6 out of 8 trails), 6 of them cannot move down successfully.

the design of FDT and used as a tool of decreasing the actuation time. Also, the overall

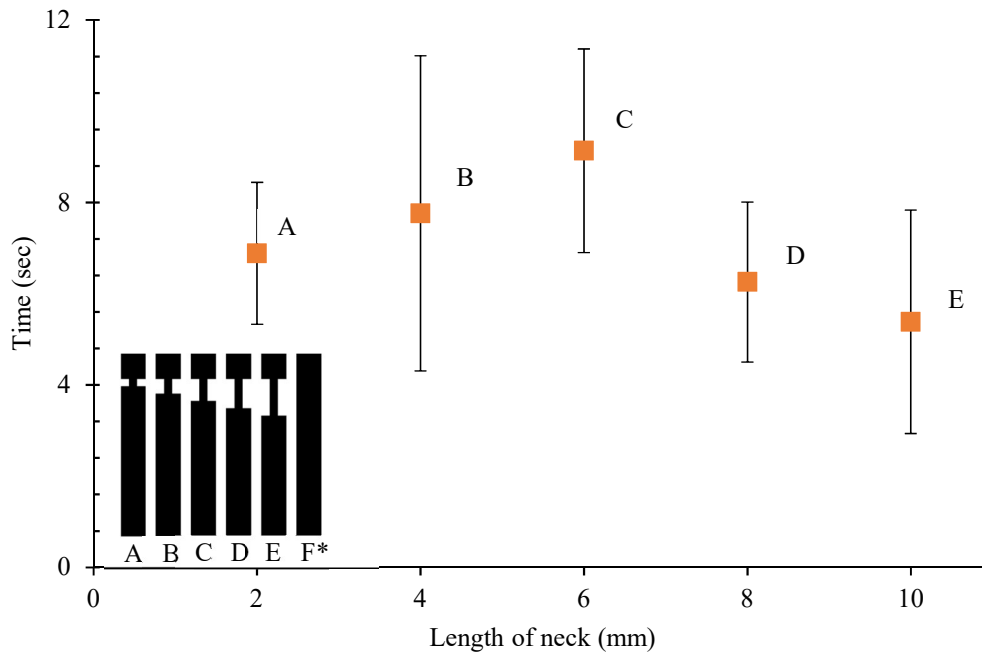


Figure 31. The length of neck of FDT in a fixed width of neck V.S. actuation time. A~E with the neck length from 2mm, 4mm, 6mm, 8mm, 10mm and F the control without the neck. The overall length for the FDT is 60mm. These shows that there is no significant relationship between the length of neck and the actuation time. *100% failure rate.

length in the group of w/o neck can be one of the parameters to adjust the actuation time. After this experiment, it can be understood that the neck can change the actuation time of FDT versus glass fiber materials without this neck structure. In the next step, we planned to test if the width or the length of the neck could change the actuation time. We varied the length of the neck from 2mm, 4mm, 6mm, 8mm and 10mm at a fixed width of 2mm (Figure 31). There was no relationship between the actuation time and the length of the neck (Figure 31). Then we varied the width from 2mm, 3mm, 4mm, 5mm, and 6mm, plus the control without a neck. As the orange plot in Figure 32 shows, the neck width was proportional to the actuation time of which range was from the average of 7secs to of 55secs. Meanwhile, we had the other group with an overall length of 50mm and varied the width of neck to see what is the performance under shorter overall length. The blue

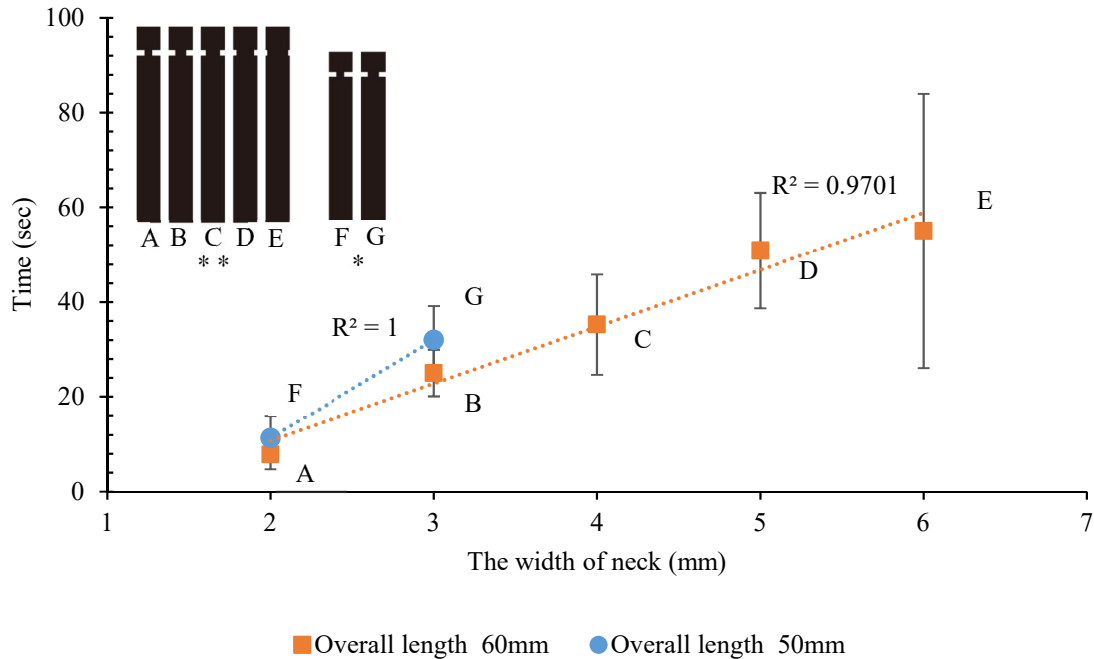


Figure 32. *Overall length 50mm, neck width in 4, 5, 6 and no neck, success rate for all is 0% (n=8) ** The group of overall lengths of 60mm w/o neck success rate is 37.5%, average time: 187.6 secs (n=8) plot in Figure 32 showed that the width of the neck is still proportional to the actuation time. However, as the width of neck increased from 4mm to 6mm and even with no neck in the group of 50mm overall length, the failure rate was 100% (n=8 for each neck width set, we were not able to make a plot from that). Based upon these results, we believed that the width of the neck and the overall length (or the proportion of FDT) can be adjusted for vary the actuation time. The overall length of FDT changed is adjusting the weight of FDT and the maximum weight of fluid the FDT can wick.

3.1.3. Combination of 2-Dimensions and 3-Dimensions Control Strategies

As the former two sections 3.1.1. and 3.1.2 mentioned two different strategies for changing the actuation time for the FDT. In this section, we demonstrated the combination of these two methods which can be easily used to vary the actuation time of FDT.

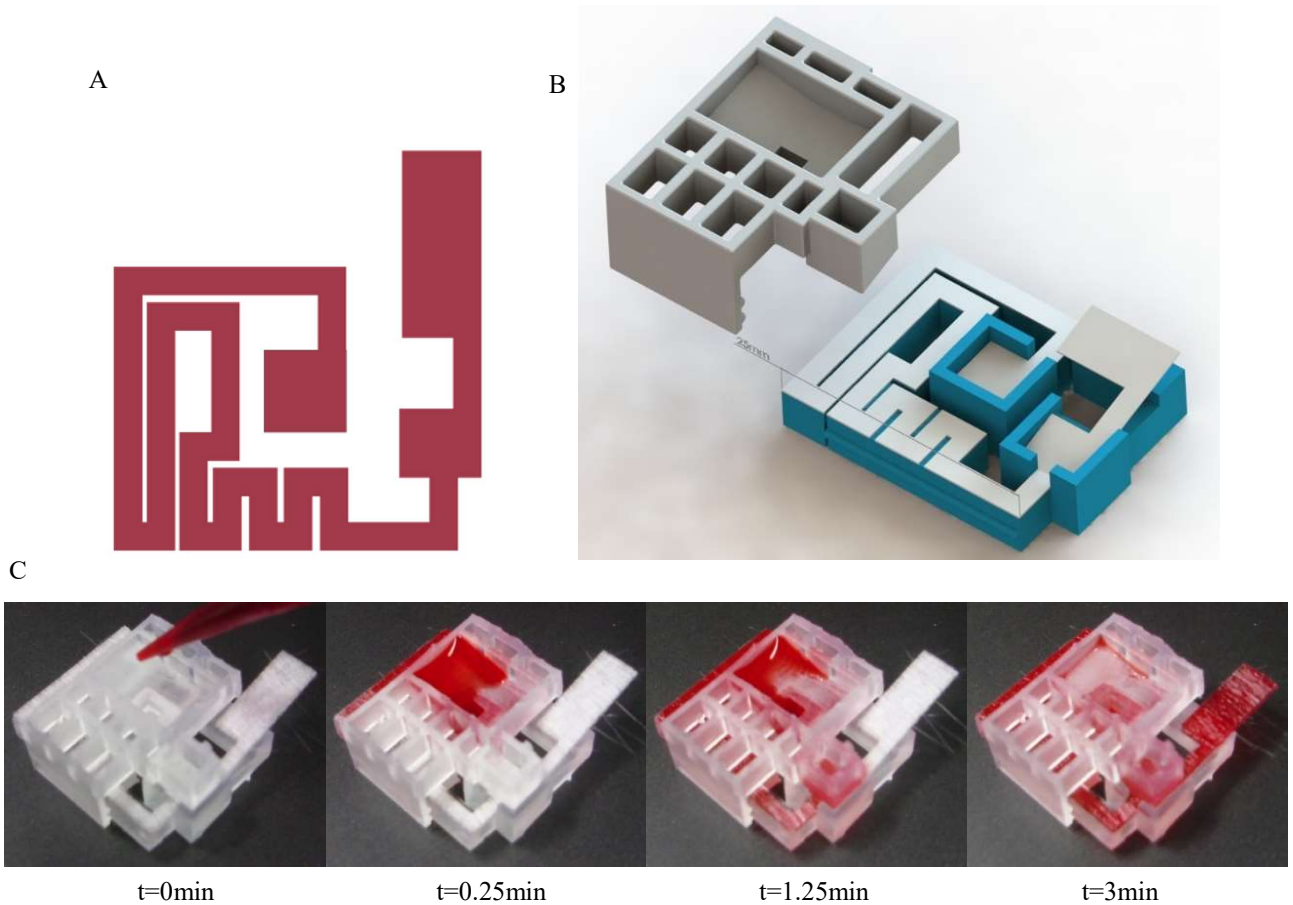


Figure 33. Prototype V1. Serpentine-based-fluidic-driven network and V1 programmable timing device. (A) The serpentine-based-fluidic-driven network. (B) The grey/white upper part is the lid of programmable timing device, included functional parts, reservoir (capacity of $\sim 250\mu\text{L}$), FDT pressure pillar and two hasps for fixing the lid to the bottom and for making good contact between the reservoir and SBCDN. (C) The time lapse pics of the process of SBCDN actuation. The FDT moved down after 3min.

Toward this goal, we used a serpentine timing structure which takes less space than the straight one connected with the FDT (Figure 33 A). This serpentine-based-fluidic-driven network (SBCDN) was made from glass fiber and fabricated by a laser

cutter in a bed volume of $194\mu\text{L}/\text{cm}^2$ with 130mm in overall length. Meanwhile, we designed a programmable timing device with a reservoir for introducing fluid and the base for supporting the SBCDN for successfully running the experiment (Figure 33 B). We set up a small timing network with an expected delay time to actuation of 3min. For reducing the size of the network, we decreased the width of the neck cross section to 2mm. Using food dye to visualize the fluids as they travel through the SBCDN (Figure 33C), the travel time through the serpentine network was approximately 1.25min followed by a drop of the FDT at 3min as expected. Therefore, we can use the SBCDN as the main timing network and the FDT was for moving down immediately and reaching the main channel, which also can avoid the fluid in the main channel flows back into the timing network.

The previous experiment demonstrated the hypothesis that combining 2-dimension and 3-dimension geometry network can be used as a timing structure. In the next step, our purpose was to design a network with two sets of the timing device and with an entire lateral flow immunoassay system. This system had five components, including the absorbent pad, nitrocellulose membrane, SBCDN, device lid and base (Figure 34). This device was set-up for introducing three kinds of reagents, including a sample, wash buffer and signal amplification reagents. All these reagents were introducing from three reservoirs on the top of the lid. The nitrocellulose membrane was placed on the bottom where was underneath of the sample reservoir and the end of nitrocellulose was connected to the absorbent pad with a 2mm overlap. One of the SBCDN for Wash buffer with a bed volume of $194\mu\text{L}/\text{cm}^2$ (130mm in overall length)

was placed on the bottom located before the sample entrance while the other one for amplification reagents with a bed volume of $228\mu\text{L}/\text{cm}^2$ (188mm in overall length) was located after the sample entrance (Figure 34). We pipetted $100\mu\text{L}$ red food dye as the sample into the sample reservoir, $300\mu\text{L}$ yellow food dye as the wash buffer and $400\mu\text{L}$ blue food dye as a surrogate for the amplification reagents, e.g., gold enhancement (Figure 34 C). As shown in Figure 34, the delay time was 2.5min (expected 3min) for the yellow food dye to reach the main channel and 7.5min (expected 5min) for the blue dye.

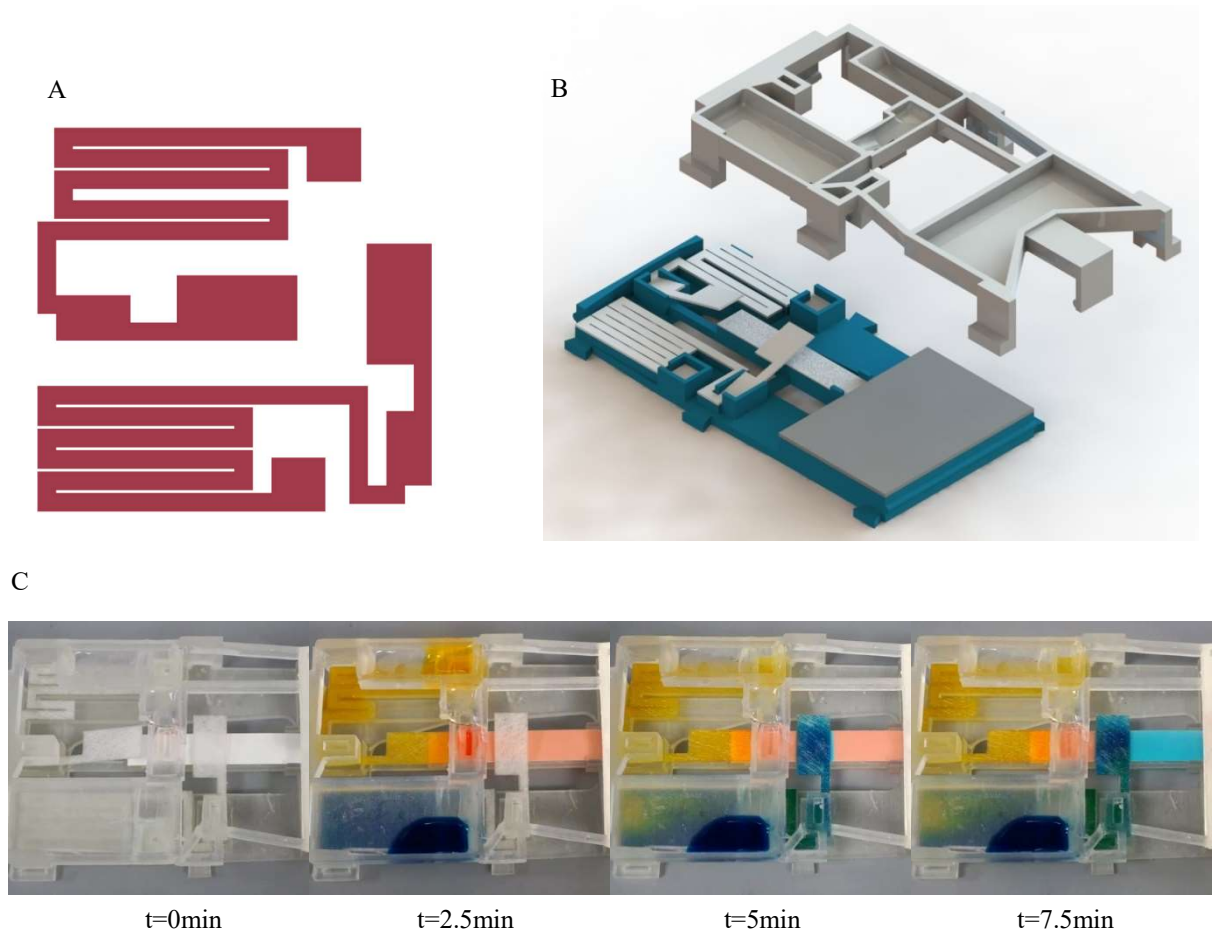


Figure 34. Prototype V2 Serpentine-based-fluidic-driven network and V2 programmable timing device. (A) The serpentine-based-fluidic-driven networks, one is lined up with the main channel and the other one is vertically placed on the main channel. (B) The grey/white upper part is the lid of programmable timing device, included functional parts, reservoir, the capacity for sample is $\sim 200\mu\text{L}$, for wash buffer is $500\mu\text{L}$, and for amplified reagents is $1000\mu\text{L}$, FDT pressure pillar and six clamps for fixing the lid to the bottom and for making good contact between the reservoir and SBCDN. (C) The time lapse pics of the process of SBCDN actuation. The 1st FDT moved down by 2.5min and the 2nd moved down by 5min.

However, the yellow food dye was not able to flow through the tube that connected the reservoir to the nitrocellulose membrane. The tube blocked the flows from the first SBCDN. Moreover, the asymmetrical FDT did not work very well (2 out of 3 was failed, n=3). Thus, we needed to change the location of the first SBCDN and reduce the width of FDT's neck.

In the next prototype version, we placed the first SBCDN after the sample reservoir (Figure 35). We expected the 3rd version of PTD would have a timing actuation time for washing buffer was 3min and for amplified reagents was 5min (Figure 35). As the result, the actuation time of the 1st SBCDN with a bed volume of $212\mu\text{L}/\text{cm}^2$ (130mm in overall length) was 2.5min delayed (2/3 failure rate, n=3) and of the 2nd one with a bed volume of $289\mu\text{L}/\text{cm}^2$ (195mm in overall length) was 5min delayed (2/3 failure rate, n=3). However, there were two issues occurred. One was the leakage between the

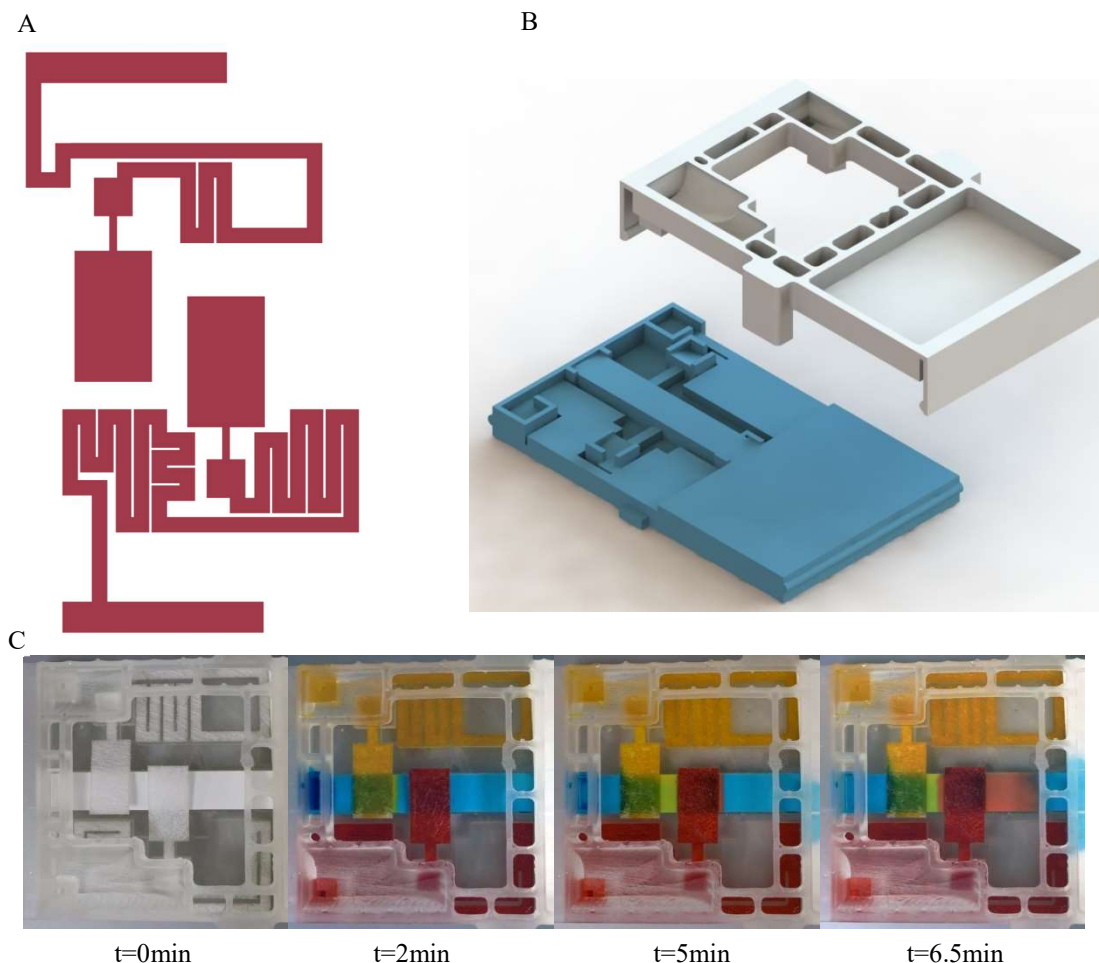


Figure 35. Prototype V3 Serpentine-based-fluidic-driven network and V3 programmable timing device. (A) The serpentine-based-fluidic-driven networks, both are vertically placed on the main channel. (B) The grey/white upper part is the lid of programmable timing device, included functional parts, reservoir, the capacity for sample is $\sim 200\mu\text{L}$, for wash buffer is $500\mu\text{L}$, and for amplified reagents is $1000\mu\text{L}$, FDT pressure pillar and six clamps for fixing the lid to the bottom and for making good contact between the reservoir and SBCDN. (C) The time lapse pics of the process of SBCDN actuation. The 1st FDT moved down by 2min and the 2nd moved down by 5min.

reservoirs and the SBCDN. The other issue was different pressure occurred due to a different volume of reagents in different reservoirs. These variable pressures from different reservoirs had an impact on the actuation time based on the Washburn equation. It turned out that the experimental actuation time observed deviated from our predictions based upon the Washburn equation. Additionally, the 2mm width neck was too wide for a short length of the first segment of the FDT moving down successfully and caused the failure rate of FDT moving down was high. Therefore, we decided to adjust two

structures, one was for the SBCDN decreasing the neck width and the other was placing the reservoirs in parallel for the SBCDN on the same level of SBCDN to avoid causing pressure from the different volume of reagents.

In the 4th version of PTD, we decreased the neck width from 2 mm to 1 mm (Figure 36 A) and the two reservoirs were placed at the same level of the bottom, each of reservoir can contain 1000 μ L reagents at maximum (Figure 36 B). The space of SBCDN for both wash buffer and amplification reagents can have a \sim 5min timing network at last. In this experiment, our purpose was to have a 3min timing delay for wash buffer flowing through from reservoir to get into the main channel; and had a 5min timing delay for amplified reagents moving from the reservoir into the main channel. The bed volume for the 1st SBCDN was 212 μ L/cm² (130mm in overall length) and the 2nd one was 289 μ L/cm² (195mm in overall length). In the first step, we tested this device and network by flowing food dye to see if the pressure issue still occurs. The results shown in Figure 36 C, demonstrate that the new design of PTD worked better than the 3rd version, the pressure issue has been solved. Also, the failure rate for FDT moving down was decreased to 1/3, n=3. In the second step, we decided to do the practical test with Norovirus virus like particles (VLPs) as the target pathogen. We had already embedded capture antibodies, goat anti-mouse antibodies, and anti-norovirus antibodies, onto the nitrocellulose membrane using previously established protocols (unpublished data). The GAM was present for showing if this test runs correctly while the anti-norovirus antibody was to present to identify if the sample contained the target pathogen of interest, i.e. Norovirus. We pipetted 100 μ L pre-mix VLPs reagents contained, detecting anti-norovirus antibodies conjugated with gold nanoparticles and Norovirus VLPs in the

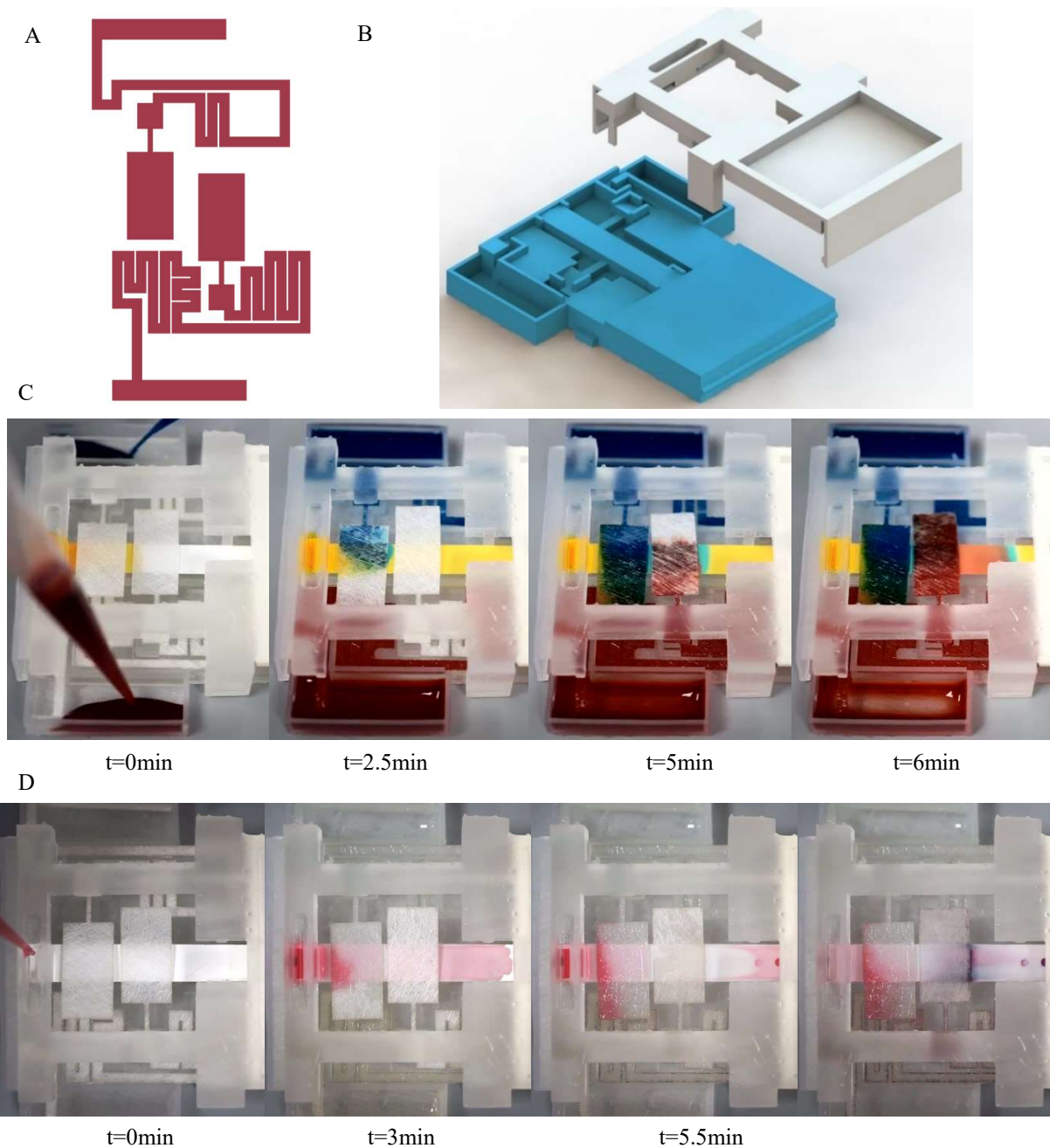


Figure 36. Prototype V4 Serpentine-based-fluidic-driven network and V4 programmable timing device. (A) The serpentine-based-fluidic-driven networks, both are vertically placed on the main channel. The neck width of the FDT has been reduced to 1mm. (B) The grey/white upper part is the lid of programmable timing device, included functional parts, reservoirs, the capacity for sample is $\sim 150\mu\text{L}$, for wash buffer is $1000\mu\text{L}$, and for amplified reagents is $1000\mu\text{L}$, FDT pressure pillar and 4 clamps for fixing the lid to the bottom and for making good contact between the reservoir and SBCDN. (C) The time lapse pics of the process of SBCDN actuation. The 1st FDT moved down by 3min and the 2nd moved down by 5.5min.

sample reservoir. Meanwhile, we introduced wash buffer and the gold enhancement

reagents into the other two reservoirs. As seen in Figure 36, after the sample was injected

into the sample reservoir, it flowed into the nitrocellulose membrane from the reservoir and reached the detection area binding with the capture antibodies to show the positive signal at both the Norovirus capture spot and the positive control GAM spot. Therefore, the 4th version of PTD can run a complete lateral flow immunoassay and generate positive signals in the presence of the target pathogen. However, one issue was the actuation time for wash buffer was too short to let all the sample flow through and reach the detection area. Before all the sample has been depleted the first SBCDN actuated and connected to the main channel. The wash buffer cut off the sample flow, thus not all the sample could make a reaction with the capture antibodies. The other issue was the second SBCDN actuated too fast, the actuation time gap between the first and the second SBCDN needed to be increased to avoid the situation that only a small volume of wash buffer could reach the detection area before the second SBCDN connected with the main channel. This prevented the background from being cleaned off completely by enough wash buffer. Therefore, we again needed to change the actuation time of the timing network.

In the 5th version of PTD, we increased the length of SBCDN and FDT in order to have a longer actuation time and a success rate for actuating the SBCDN, respectively (Figure 37 A). The bed volume of 1st SBCDN was $320\mu\text{L}/\text{cm}^2$ (216mm in overall length) and of 2nd one was $389\mu\text{L}/\text{cm}^2$ (275mm in overall length). Meanwhile, we also added

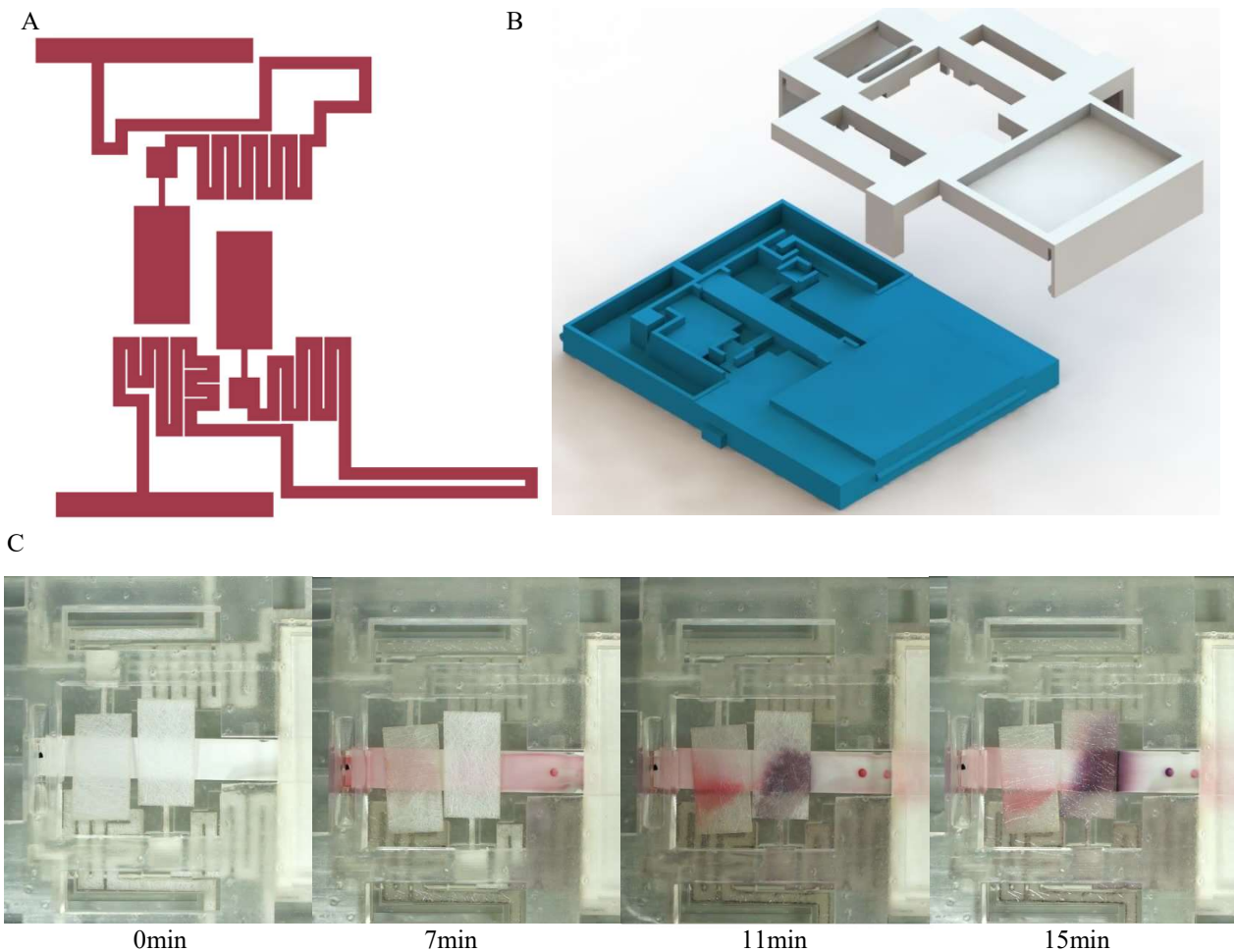


Figure 37. Prototype V5 Serpentine-based-fluidic-driven network and V5 programmable timing device. (A) The serpentine-based-fluidic-driven networks, both are vertically placed on the main channel. The length of the first segment of SBCDN increased from 17mm to 19mm. The overall length of the first SBCDN is 220mm and the second is 290mm. (B) The grey/white upper part is the lid of programmable timing device, included functional parts, reservoirs, the capacity for sample is $\sim 150\mu\text{L}$, for wash buffer is $\sim 2300\mu\text{L}$, and for amplified reagents is $\sim 2300\mu\text{L}$, FDT pressure pillar and 4 clamps for fixing the lid to the bottom and for making good contact between the reservoir and SBCDN. (C) The time lapse pics of the process of SBCDN actuation. The 1st FDT moved down by 7min and the 2nd moved down by 11min.

more space for placing larger SBCDN (Figure 37 B). As demonstrated in Figure 37, the wash buffer reaching the main channel spent more time there, 7min versus the 3min in the 4th version. And the actuation time for gold enhancement was also increased to allow more wash buffer to push the excess fluid to the absorbent pad. There were two visible, colorimetric signals indicating that the immunoassay ran correctly and the norovirus

VLPs had been recognized by the capture antibodies (Figure 37). Therefore, we have

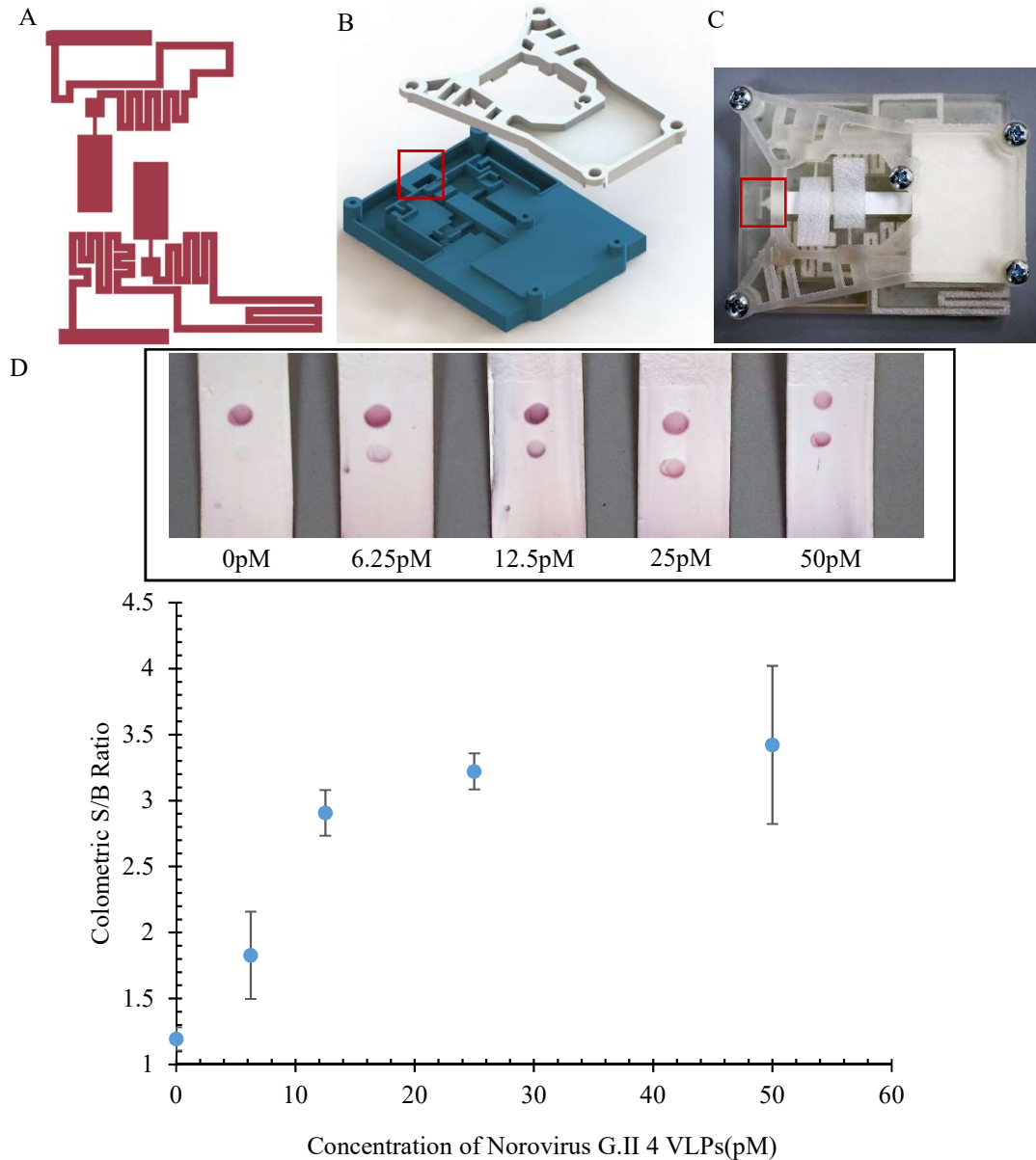


Figure 38. Prototype V6 Serpentine-based-fluidic-driven network and V6 programmable timing device. (A) The serpentine-based-fluidic-driven networks, both are vertically placed on the main channel. The overall length of the first SBCDN is 220mm and the second is 290mm. (B) The grey/white upper part is the lid of programmable timing device, included functional parts, reservoirs, the capacity for sample is $\sim 100\mu\text{L}$, for wash buffer is $\sim 2100\mu\text{L}$, and for amplified reagents is $\sim 2100\mu\text{L}$, FDT pressure pillar and 5 screw wholes for fixing the lid to the bottom and for making good contact between the reservoir and SBCDN. Also, relocating the sample reservoir to the bottom as the same level of other two reservoirs. (C) The time lapse pics of the process of SBCDN actuation. The 1st FDT moved down by $7\pm 0.5\text{min}$ and the 2nd moved down by $11\pm 0.2\text{min}$. Collaboration with Kshitij Ranjan.

demonstrated our PTD can be used for a programmable timing lateral flow immunoassay.

We can adjust the length of SBCDN for varying the actuation time for the SBCDN to change the reaction time a washing time. However, during the experiment, we found there is a leaking issue between the sample reservoir and the nitrocellulose membrane. To deal with this problem, we relocated the sample reservoir to the sample level of other two reservoirs to avoid the leaking issue from pressure difference (Figure 38 B, C).

In the 6th version of PTD, we designed five screws position for making even pressure onto the SBCDN and keeping the absorbent pad tight to the nitrocellulose membrane (Figure 38). The bed volume of 1st SBCDN was 328 μ L/cm² (220mm in overall length) and of 2nd one was 410 μ L/cm² (290mm in overall length). One small piece of glass fiber also has been dipped into the sample reservoir and the other side was

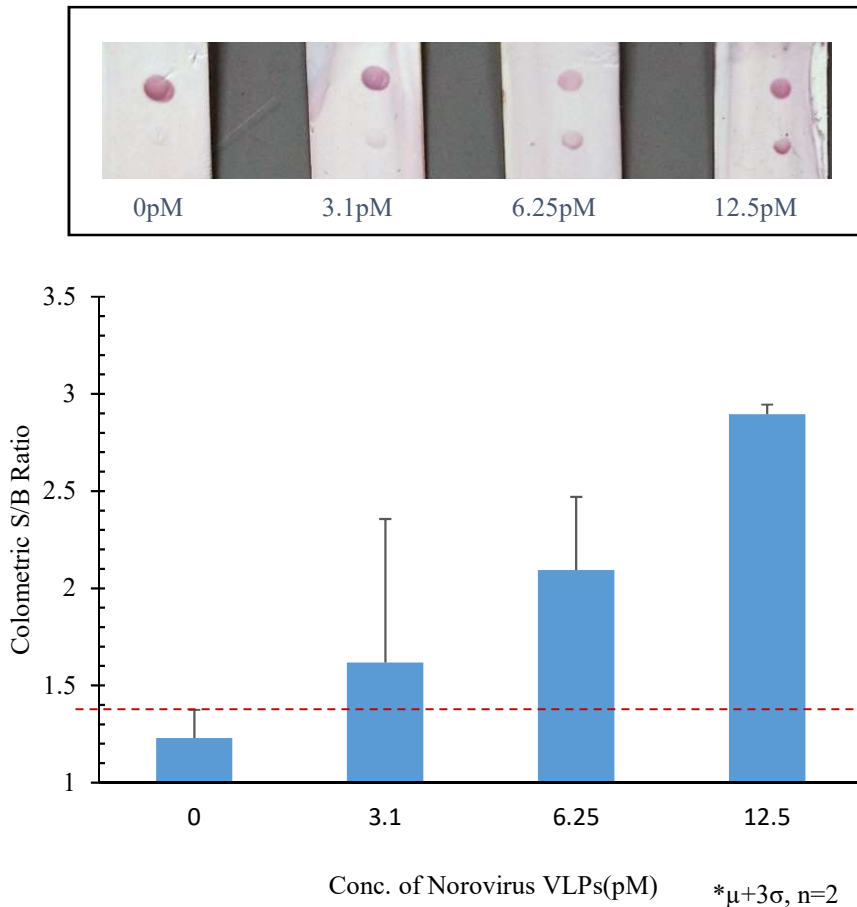


Figure 39. The dose-response experiment for Norovirus GII.4 (n=2).

overlapping with the nitrocellulose membrane for avoiding the leaking issue and keeping the flow rate of sample controllable. Upon on this design, we did two dose-response experiments with gold enhancement. The concentration range of Norovirus GII.4 is 0 as control, 6.25pM, 12.5pM, 25pM and 50pM (Figure 38). During the experiment, we introduced the 70 μ L pre-mixed sample into sample reservoir along with 700 μ L of wash buffer and of gold enhancement reagent. In the experiment, we found that the positive signal for Norovirus still presented. Thus, we decided to push the concentration down to the 3.1pM to see the limit of threshold. We designed the next dose-response experiments performing at the concentration from 0, 3.1pM, 6.25pM and 12.5pM (Figure 39). We did two replicates based on this protocol. The plot presented a standard error in $+3\sigma$. As the results shown, it appeared that the signal intensity was increasing as the concentration increased. In addition, we could demonstrate the lowest concentration of Norovirus GII.4 VLPs we could detect by our system was 6.25pM based on the current condition of 70 μ L pre-mixed sample.

4. CONCLUSIONS AND FUTURE DIRECTIONS

From my experimental results, the idea of building up of a programmable fluidic driven LFIA device for integrating with *ParatusSDS*[®] *Cartridge* has been demonstrated. To tailor the LFIA device for existing and emerging applications, we have demonstrated methods to control different parameters, such as timing and volume, of this device using both 2-dimensional and 3-dimensional patterns.

Future directions for this work will involve multi-plexing, where multiple anti-antigen capture antibodies are embedded on the nitrocellulose membrane for detecting different, but closely-related pathogens that cause similar symptoms. Preliminary arrays were demonstrated for up to 6 pathogens plus controls. This technique can be applied in the multiplexing detection for those infectious diseases which are not only caused by one type of pathogen but multiple, such as gastroenteritis. This is a key advantage of the integrated *ParatusSDS*[®] *Cartridge* and LFIA device over other traditional lateral flow immunoassays which can only detect one antigen at a time. In addition, for increasing the signal from the low concentration antigen in the sample, variable methods can be applied to our device, e.g. gold enhancement. Moreover, the fully time sequence was 20min, from sample introduction, buffer washing off the excess fluids and signal detection.

The programmable LFIA timing device described in this thesis is suitable for integration into *ParatusSDS*[®] *Cartridge* in order to ultimately generate a diagnostic system that is easy to use by one-step actuation introducing reagents and automated sequencing of all LFIA test steps. Furthermore, it is expected to contain more than two SBCDNs depending on how many reagents need to be transported to the detection area on an application-specific basis. Taken together, the work presented in this thesis provide

a basis for further timed fluidic actuation and integration of capillary-driven microfluidics into an easy-to-use, portable, multiplexed and highly sensitive detection system for differential disease diagnosis.

REFERENCES

- National Institute of Diabetes and Digestive and Kidney Diseases. "Viral Gastroenteritis." Viral Gastroenteritis Accessed September 7, 2015.
<http://digestive.niddk.nih.gov/ddiseases/pubs/viralgastroenteritis/index.htm>.
- Antibiotics Aren't Always the Answer.* (2015). Centers for Disease Control and Prevention Retrieved from <http://www.cdc.gov/Features/GetSmart/index.html>.
- Bailey, G. W., Jerome, W. G., McKernan, S., Mansfield, J. F., & Price, R. L. (1999). *Gold-Based Autometallography*. Paper presented at the Microscopy Society of America, New York, NY.
- Batchelor, G. K. (2000). *An Introduction to Fluid Dynamics*: Cambridge Mathematical Library.
- Carrilho, E., Martinez, A. W., & Whitesides, G. M. (2009). Understanding wax printing: a simple micropatterning process for paper-based microfluidics. *Anal Chem*, 81(16), 7091-7095. doi:10.1021/ac901071p
- Casburn-Jones, A. C., & Farthing, M. J. (2004). Management of infectious diarrhoea. *Gut*, 53(2), 296-305. doi:10.1136/gut.2003.022103
- CDC. (2017). Diagnostic Methods. Retrieved from <https://www.cdc.gov/norovirus/lab-testing/diagnostic.html>
- Chen, H., Cogswell, J., Anagnostopoulos, C., & Faghri, M. (2012). A fluidic diode, valves, and a sequential-loading circuit fabricated on layered paper. *Lab Chip*, 12(16), 2909-2913. doi:10.1039/c2lc20970e
- Chin, C. D., Linder, V., & Sia, S. K. (2007). Lab-on-a-chip devices for global health: past studies and future opportunities. *Lab Chip*, 7(1), 41-57. doi:10.1039/b611455e
- Daar, A. S., Thorsteinsdottir, H., Martin, D. K., Smith, A. C., Nast, S., & Singer, P. A. (2002). Top ten biotechnologies for improving health in developing countries. *Nat Genet*, 32(2), 229-232. doi:10.1038/ng1002-229
- Elliott, E. J. (2007). Acute gastroenteritis in children. *BMJ*, 334(7583), 35-40. doi:10.1136/bmj.39036.406169.80
- Fu, E., Ramsey, S. A., Kauffman, P., Lutz, B., & Yager, P. (2011). Transport in two-dimensional paper networks. *Microfluid Nanofluidics*, 10(1), 29-35. doi:10.1007/s10404-010-0643-y
- Geankoplis, C. J. (2003). *Transport Processes and Separation Process Principles*: Prentice Hall Professional Technical Reference.
- Gerbers, R., Foellscher, W., Chen, H., Anagnostopoulos, C., & Faghri, M. (2014). A new paper-based platform technology for point-of-care diagnostics. *Lab Chip*, 14(20), 4042-4049. doi:10.1039/c4lc00786g
- Gere, J. M. G., Barry J. (2012). *Mechanics of Materials* (Eighth ed.).
- Gill, C. J., Lau, J., Gorbach, S. L., & Hamer, D. H. (2003). Diagnostic accuracy of stool assays for inflammatory bacterial gastroenteritis in developed and resource-poor countries. *Clin Infect Dis*, 37(3), 365-375. doi:10.1086/375896
- Hainfeld, J., & Powell, R. (2002). Silver- and Gold-Based Autometallography of Nanogold. *Gold and Silver Staining Advances in Pathology, Microscopy, & Molecular Morphology Techniques in Molecular Morphology*, 20020461, 29-46. doi:10.1201/9781420040234.ch3

- Hines, J., & Nachamkin, I. (1996). Effective Use of the Clinical Microbiology Laboratory for Diagnosing Diarrheal Diseases *Clin Infect Dis*, 23, 1292-1301.
- Holt, J. G., Krieg, N. R., Sneath, P. H. A., Staley, J. T., & Williams, S. T. (1994). *Bergey's Manual of Determinative Bacteriology* (9 ed.): Lippincott Williams & Wilkins.
- Iijima, Y., Tanaka, S., Miki, K., Kanamori, S., Toyokawa, M., & Asari, S. (2007). Evaluation of colony-based examinations of diarrheagenic *Escherichia coli* in stool specimens: low probability of detection because of low concentrations, particularly during the early stage of gastroenteritis. *Diagn Microbiol Infect Dis*, 58(3), 303-308. doi:10.1016/j.diagmicrobio.2007.02.007
- Jamison, D. T. (2006). *Disease control priorities in developing countries*. New York: Oxford University Press.
- Lozano, R., Naghavi, M., Foreman, K., Lim, S., Shibuya, K., Aboyans, V., . . . Memish, Z. A. (2012). Global and regional mortality from 235 causes of death for 20 age groups in 1990 and 2010: a systematic analysis for the Global Burden of Disease Study 2010. *Lancet*, 380(9859), 2095-2128. doi:10.1016/S0140-6736(12)61728-0
- Lutz, B., Liang, T., Fu, E., Ramachandran, S., Kauffman, P., & Yager, P. (2013). Dissolvable fluidic time delays for programming multi-step assays in instrument-free paper diagnostics. *Lab Chip*, 13(14), 2840-2847. doi:10.1039/c3lc50178g
- Lutz, B. R., Trinh, P., Ball, C., Fu, E., & Yager, P. (2011). Two-dimensional paper networks: programmable fluidic disconnects for multi-step processes in shaped paper. *Lab Chip*, 11(24), 4274-4278. doi:10.1039/c1lc20758j
- Mabey, D., Peeling, R. W., Ustianowski, A., & Perkins, M. D. (2004). Diagnostics for the developing world. *Nat Rev Microbiol*, 2(3), 231-240. doi:10.1038/nrmicro841
- Mandell, G. L., John, B., & Dolin, R. (2010). *Mandell, Douglas, and Bennett's principles and practice of infectious diseases*. Philadelphia, PA: Churchill Livingstone/Elsevier.
- Martinez, A. W., Phillips, S. T., Whitesides, G. M., & Carrilho, E. (2010). Diagnostics for the developing world: microfluidic paper-based analytical devices. *Anal Chem*, 82(1), 3-10. doi:10.1021/ac9013989
- N. Kurn, R. D. P., M. Becker and E. F. Ullman. (1992). Device and method for interrupting capillary flow. 5104812.
- Nimunkar, A., Baran, J., Van Sickle, D., & Webster, J. G. (2009). *Medical devices for developing countries: Design constraints and approaches*. Paper presented at the Annual International Conference of the IEEE Engineering in Medicine and Biology Society.
- Pawlowski, S. W., Warren, C. A., & Guerrant, R. (2009). Diagnosis and treatment of acute or persistent diarrhea. *Gastroenterology*, 136(6), 1874-1886. doi:10.1053/j.gastro.2009.02.072
- Peek, R. L., and D. A. Mclean. (1934). Capillary Penetration of Fibrous Materials. *Ind Eng Chem*, 6(2), 85-90.
- Peeling, R. W., Holmes, K. K., Mabey, D., & Ronald, A. (2006). Rapid tests for sexually transmitted infections (STIs): the way forward. *Sex Transm Infect*, 82 Suppl 5, v1-6. doi:10.1136/sti.2006.024265
- Posthuma-Trumpie, G. A., Korf, J., & van Amerongen, A. (2009). Lateral flow (immuno)assay: its strengths, weaknesses, opportunities and threats. A literature survey. *Anal Bioanal Chem*, 393(2), 569-582. doi:10.1007/s00216-008-2287-2

- R. A. Bunce, G. H. G. H. T., J. E. C. Gibbons, L. J. Keen, & Walker, a. M. R. (1993). Liquid transfer device. 5198193.
- R. D. Patel, N. K., M. Becker and E. F. Ullman. (1992). Device and method for completing a fluidic circuit which employs a liquid expandable piece of bibulous material. 5135873.
- Rambau, P. F. (2011). Pathology Practice in a Resource-Poor Setting: Mwanza, Tanzania. *Archives of Pathology & Laboratory Medicine*, 135(2), 191-193. doi:doi:10.1043/1543-2165-135.2.191
- Rohde, R., & Weigum, S. (2017). Nucleic Acid-Based Analytic Methods for Microbial Identification and Characterization. In Bailey & Scott (Eds.), *Diagnostic Microbiology* (14th ed.): Elsevier.
- Saha, K., Agasti, S. S., Kim, C., Li, X., & Rotello, V. M. (2012). Gold nanoparticles in chemical and biological sensing. *Chem Rev*, 112(5), 2739-2779. doi:10.1021/cr2001178
- Sharma, H., Nguyen, D., Chen, A., Lew, V., & Khine, M. (2011). Unconventional low-cost fabrication and patterning techniques for point of care diagnostics. *Ann Biomed Eng*, 39(4), 1313-1327. doi:10.1007/s10439-010-0213-1
- Sia, S. K., Linder, V., Parviz, B. A., Siegel, A., & Whitesides, G. M. (2004). An integrated approach to a portable and low-cost immunoassay for resource-poor settings. *Angew Chem Int Ed Engl*, 43(4), 498-502. doi:10.1002/anie.200353016
- Sidoti, F., Ritta, M., Costa, C., & Cavallo, R. (2015). Diagnosis of viral gastroenteritis: limits and potential of currently available procedures. *J Infect Dev Ctries*, 9(6), 551-561. doi:10.3855/jidc.7051
- Sirajuddin, Mechler, A., Torriero, A. A. J., Nafady, A., Lee, C.-Y., Bond, A. M., . . . Bhargava, S. K. (2010). The formation of gold nanoparticles using hydroquinone as a reducing agent through a localized pH change upon addition of NaOH to a solution of HAuCl₄. *Colloids and Surfaces A: Physicochemical and Engineering Aspects*, 370(1-3), 35-41. doi:10.1016/j.colsurfa.2010.08.041
- Songjaroen, T., Dungchai, W., Chailapakul, O., & Laiwattanapaisal, W. (2011). Novel, simple and low-cost alternative method for fabrication of paper-based microfluidics by wax dipping. *Talanta*, 85(5), 2587-2593. doi:10.1016/j.talanta.2011.08.024
- SV, K., WJ, S., PA, R., A, Z., J, B., D, L., . . . SB, H. (2003). Fecal lactoferrin is a sensitive and specific marker in identifying intestinal inflammation. *Am J Gastroenterol*, 98(6), 1309-1315.
- Toley, B. J., McKenzie, B., Liang, T., Buser, J. R., Yager, P., & Fu, E. (2013). Tunable-delay shunts for paper microfluidic devices. *Anal Chem*, 85(23), 11545-11552. doi:10.1021/ac4030939
- Toley, B. J., Wang, J. A., Gupta, M., Buser, J. R., Lafleur, L. K., Lutz, B. R., . . . Yager, P. (2015). A versatile valving toolkit for automating fluidic operations in paper microfluidic devices. *Lab Chip*, 15(6), 1432-1444. doi:10.1039/c4lc01155d
- Washburn, E. W. (1921). The Dynamics of Capillary Flow. *Physical Review*, 17(3), 273-283. doi:10.1103/PhysRev.17.273
- Webber, R. (2005). *Communicable Disease Epidemiology and Control*. Cambridge, MA: CABI Pub.
- White, A. C., Jr. (2010). *Cryptosporidiosis (Cryptosporidium hominis, Cryptosporidium parvum and Other species)*: Churchill Livingstone.

- Williams, R. (1981). the capillary without wall. *Journal of Colloid and Interface Science*, 79(1). doi:10.1016/0021-9797(81)90074-6
- Yager, P., Edwards, T., Fu, E., Helton, K., Nelson, K., Tam, M. R., & Weigl, B. H. (2006). Microfluidic diagnostic technologies for global public health. *Nature*, 442(7101), 412-418. doi:10.1038/nature05064